

TOPICAL REVIEW • OPEN ACCESS

Resonant states and their role in nanophotonics

To cite this article: S Both and T Weiss 2022 *Semicond. Sci. Technol.* **37** 013002

View the [article online](#) for updates and enhancements.

You may also like

- [Resonant states in double and triple quantum wells](#)
A Tanimu and E A Muljarov
- [Information physics fundamentals of nanophotonics](#)
Makoto Naruse, Naoya Tate, Masashi Aono et al.
- [Probing the resonance of Dirac particle in the relativistic point-coupling model by complex-momentum-representation method](#)
Y Wang, , Z M Niu et al.



IOP | ebooks™

Bringing together innovative digital publishing with leading authors from the global scientific community.

Start exploring the collection—download the first chapter of every title for free.

Topical Review

Resonant states and their role in nanophotonics

S Both¹  and T Weiss^{1,2,*} ¹ 4th Physics Institute and SCoPE, Pfaffenwaldring 57, 70569 Stuttgart, Germany² Institute of Physics, University of Graz, and NAWI Graz, Universitätsplatz 5, 8010 Graz, AustriaE-mail: thomas.weiss@uni-graz.at

Received 1 July 2021, revised 8 October 2021

Accepted for publication 22 October 2021

Published 6 December 2021



CrossMark

Abstract

Resonant phenomena have been extensively used in micro- and nanophotonics. Mathematically, these phenomena originate in a discrete set of basis functions known as resonant states or quasi-normal modes. Therefore, it is extremely beneficial to develop theoretical approaches that use these resonant states as a physically meaningful basis in order to describe the light–matter interaction in micro- and nanoresonators. However, the question of how to normalize resonant states correctly for such an expansion initially hampered many theoretical attempts. Only recently, this problem of normalization has been solved via different approaches, providing a completely rigorous basis for not only explaining but also quantifying a large variety of resonant phenomena. This review article provides an overview of the related activities in the field and typical applications. We compare the different approaches with a focus on formulations via the Mittag-Leffler expansion of the Green’s dyadic on the complex frequency plane and an analytic normalization scheme for the resonant states. Specifically, we discuss the pole expansion of the near and far field and outline related theoretical tools such as the resonant-state expansion and first-order perturbation theories. These approaches allow for efficiently describing light–matter interaction between local emitters and resonators, scattering of light at nanoparticles, and resonantly-enhanced optical sensing. Moreover, the resulting equations provide insight into the underlying physical mechanisms, which can be used to tailor the light–matter interaction and to predict new phenomena such as the recently observed complex-valued mode volumes. Since the Mittag-Leffler theorem is valid beyond the continuation of physical quantities to the complex frequency plane, an introduction to alternative modal approaches, namely those based on permittivity eigenmodes and propagating modes, is included here as well. While the link of these approaches to resonant phenomena is less obvious, they can be advantageous in some cases. Finally, we show that modal theories can be even applied in nonlinear optics. Hence, the theory of resonant states provides a general theoretical framework in micro- and nanophotonics.

Keywords: nanophotonics, resonant states, quasi-normal modes

(Some figures may appear in colour only in the online journal)

* Author to whom any correspondence should be addressed.



Original Content from this work may be used under the terms of the [Creative Commons Attribution 4.0 licence](https://creativecommons.org/licenses/by/4.0/). Any further distribution of this work must maintain attribution to the author(s) and the title of the work, journal citation and DOI.

1. Introduction

The theory of resonant states (RS) in nanophotonics has attracted a lot of interest in recent years. It has been applied to various systems such as single nanoantennas [1–10], photonic crystals [11–15], waveguides [16, 17], and cavities [18–20] to describe multitudinous effects such as the interaction of emitters with resonators [2, 3, 7], light scattering [9, 13, 21–23], and sensing [11, 14, 24–27].

RS are also known as quasi-normal modes. Sometimes, they are simply termed as modes or resonances. In fact, all these expressions can be used equivalently, with the term quasi-normal modes arising probably the first time for describing tapered fibers [28], later reframed in the context of damped mechanical oscillators [29] and stellar models [30]. In contrast, the term RS stems from quantum theory and scattering at nuclei [31].

The strength of the theory of RS is to describe resonant phenomena. From a physical point of view, resonant phenomena in nanophotonics can have different origins. An overview over various resonant systems is given in figure 1. Common to all systems is some mechanism to confine light in a localized region in space. It turns out that this confinement becomes significantly amplified at certain resonance frequencies. Often, it is possible to identify a scaling behavior of the resonance frequencies with some geometrical parameters. In many cases, the scaling is linear and can be interpreted as the result of constructive interference. A prominent example is that of a whispering gallery mode [32], where light is confined inside a material with high refractive index by total internal reflection at the boundary to a low-index surrounding. This results in constructive interference of light at the resonance frequencies after one roundtrip. For instance, the resonance frequency scales linearly with the radius in spherical geometries. Owing to their narrow linewidth, whispering gallery resonances are often used in sensing devices [24, 32–34], see figure 1(a). Another important resonator type is based on collective electron oscillations, so-called surface-plasmon polaritons, see [35] and references therein. When these surface-plasmon polaritons are bound to a finite geometry as depicted in figure 1(b), they form localized plasmon resonances with very large field enhancements in localized hotspot regions [36–42]. Panel (c) in figure 1 displays pairs of gold spheres—so-called dimers—fabricated by the DNA origami technique [43]. In that experiment, a fluorophore molecule walks autonomously into the electromagnetic hotspot between the spheres, which can be detected optically as a reduction of the fluorescence lifetime. Alternatively, light can be confined by regions with photonic bandgaps that arise in photonic crystals [44–46]. An example of a photonic crystal cavity is shown in figure 1(d) [19]. More recently, high-index dielectric nanoresonators have been investigated that support Mie resonances [47–51]. Their advantage is a reduced loss compared to plasmonic nanoresonators combined with a high flexibility to tailor the interaction of different electric and magnetic resonances, see schematics and results in figures 1(e)–(g).

Resonant states can be categorized by carrying out a multipolar decomposition [52]. This yields three different

contributions with typical near- and far-field properties: electric, magnetic, and toroidal multipoles [53–55]. Often, only the lowest-order multipoles suffice to gain a better understanding of the underlying physics. For instance, the interference of toroidal and electric dipoles may lead to the occurrence of anapoles, which are nonradiating charge-current configurations that have been described in various systems [56–58].

Mathematically speaking, RS constitute eigensolutions of a set of differential equations at complex-valued eigenfrequencies that decay in time while exhibiting outgoing boundary conditions outside a resonator geometry. One may wonder about the fact that the eigenfrequencies are in general not real numbers, while experimental observations are only carried out at real frequencies. What is then the implication of these RS at complex eigenfrequencies? As a picturesque analogy, consider an old alley, where trees are planted on one side of the road. If the roots of the trees have been growing below the bitumen, the road is no longer plain. Therefore, one feels the impact of the nearby trees, albeit staying always on the road. The same holds for RS. They typically occur at frequencies with negative imaginary parts, with few exceptions such as the exotic bound states in the continuum that have a real-valued eigenfrequency [59–65]. Particularly those RS with eigenfrequencies close to the real axis can have significant impact on the optical response at real frequencies. From a physical perspective, RS oscillate in time with the real part of the eigenfrequency, while twice the magnitude of the imaginary part corresponds to the decay rate in time domain and the resonance linewidth in frequency domain. The decay in time happens due to two possible loss channels: Intrinsic losses in the materials and radiation to the exterior.

While anapoles suppress the far-field radiation only at certain frequencies due to the interplay of two RS, bound states in the continuum are RS that do not couple to the far-field at all. They can be classified as symmetry-protected and accidental bound states in the continuum [61, 66]. The former can be found whenever the coupling with the far field is forbidden by symmetry constraints of the geometry and the incoming light, which can be, e.g. achieved in photonic crystal slabs [67]. In the latter case, we can understand the origin of the nonradiative properties by the coupling of two or more RS, which may yield a zero resonant linewidth under certain ‘accidental’ conditions. Another interesting phenomenon that is attributed to the coupling of RS in open resonators is that of exceptional points [24, 68–70], where minimum two eigenstates in a system coalesce in field distribution and frequency. Finally, the arrangement of several resonators in periodic arrays also yields intriguing effects such as narrow surface-lattice resonances [71–74]. In that case, the interaction of the individual resonators is mediated by plane waves close to their diffraction opening, which is known as Rayleigh–Wood anomalies [75–77]. This interplay may result in extremely sharp spectral features that can be used, e.g. in optical sensors [40].

As discussed above, RS exhibit complex eigenfrequencies with typically nonzero imaginary parts. If the negative imaginary part of the eigenfrequencies can be partially associated to radiative losses, this results in the peculiar behavior that the eigensolutions grow with distance to the

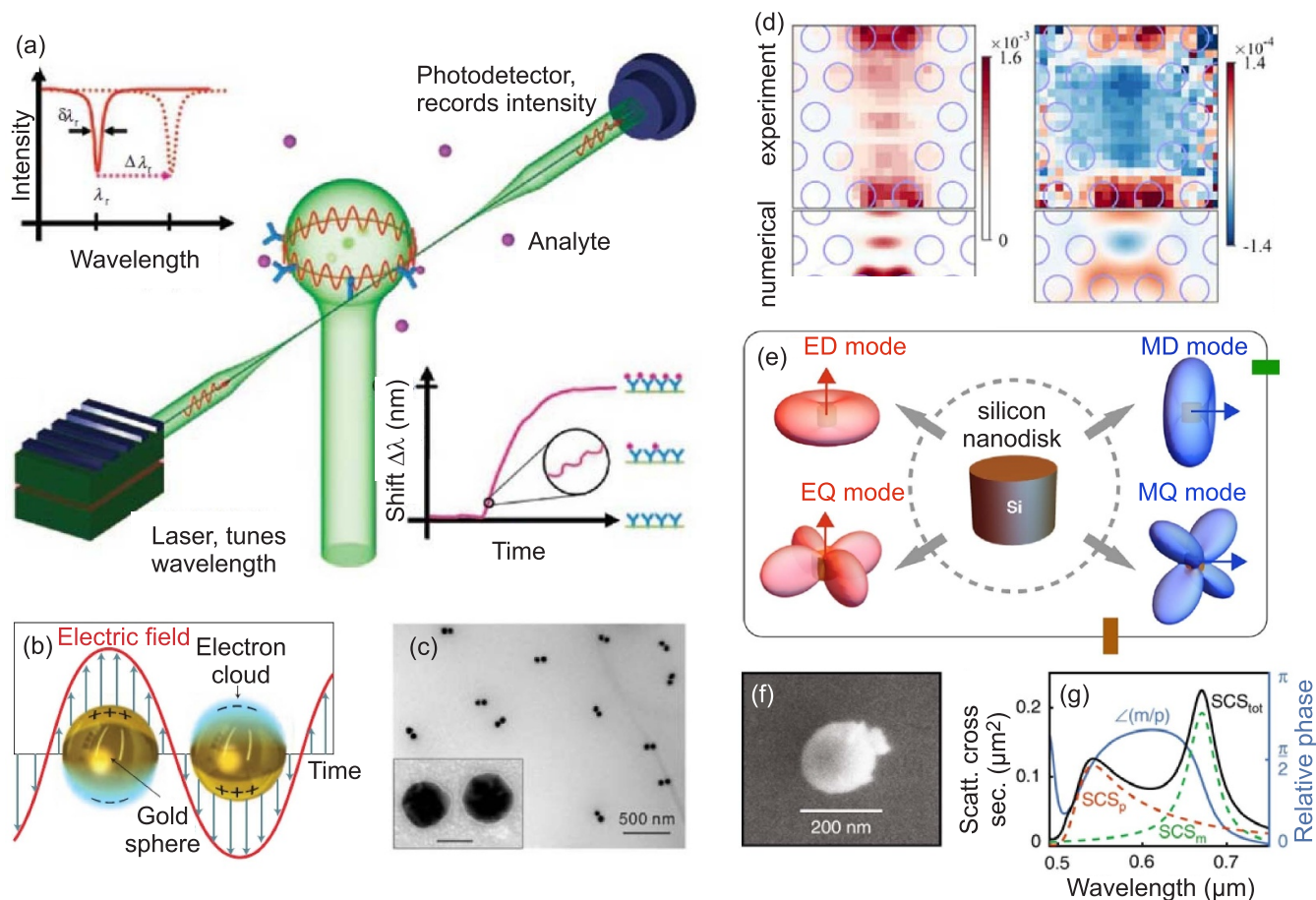


Figure 1. Examples of different resonant phenomena: (a) dielectric sphere supporting whispering gallery resonances for sensing applications. Reprinted by permission from Springer Nature Customer Service Centre GmbH: Springer Nature, *Nature Methods*, Whispering-gallery-mode biosensing: label-free detection down to single molecules, Frank Vollmer *et al.*, Copyright © 2008; (b) plasmonic resonances in single gold spheres. Reprinted by permission from Springer Nature Customer Service Centre GmbH: Springer Nature, *Nature Photonics*, Plasmon nano-optical tweezers, Mathieu L Juan *et al.*, Copyright © 2011. (c) experimental realization of plasmonic resonances in gold dimers fabricated by DNA origami technique. Reprinted with permission from [43]. Copyright (2019) American Chemical Society; (d) real (left) and imaginary (right) part of the inverse mode volume in a photonic crystal cavity. Reprinted with permission from [19] © The Optical Society; (e) electric dipolar (ED), electric quadrupolar (EQ), magnetic dipolar (MD), and magnetic quadrupolar (MQ) Mie resonances in dielectric disks. Reprinted with permission from [51]. Copyright (2021) American Chemical Society; (f), (g) SEM image and scattering cross section (SCS) for a silicon sphere with the total cross section in black, the electric and magnetic contributions in orange and green, respectively, and the relative phase between the resonances in blue. Reproduced from [50]. CC BY 4.0.

resonator. The physical explanation is that light further away from the resonator has left the resonator at a time at which more energy had been stored inside the resonator. As a consequence, conventional normalization schemes for these eigensolutions fail. However, the absence of a suitable normalization would render any theory of RS to be purely phenomenological. Several alternative approaches have been developed to solve this problem for quantum mechanics [78–80] and later applied to propagating modes in optical waveguides [81–84] and RS in optical resonators [1–3, 5–7, 11, 12, 17, 85–91]. Owing to this plethora of different formulations, the question of how to correctly normalize RS was debated a lot in recent years [90, 92, 93]. Predominantly two normalization schemes became widely accepted: (1) analytic normalizations and (2) the application of complex coordinate transformations, which is equivalent to using so-called perfectly-matched layers for the mode normalization [3]. Interestingly, it appears that those authors who are using the term quasi-normal modes prefer the

latter approach. In contrast, the term RS is mainly used in the context of analytic normalization schemes [1, 91]. While previous reviews in the field have been written from the perspective of quasi-normal modes [94, 95], this review of the theory of RS therefore sheds a slightly different light on the topic. We focus on analytic normalization schemes and the derivation of the resonant expansion via the Mittag-Leffler theorem, which can be applied to the Green's dyadic.

Another relevant aspect that deserves a broader discussion is how to derive the RS of a perturbed system based on the RS of an unperturbed reference system, which is known as the resonant-state expansion. Originally, the term resonant-state expansion was used in quantum mechanics for a general expansion of functions or operators in terms of RS [96, 97], but later refined to a perturbation theory in all orders by the Muljarov group [1, 91, 98]. In general, this perturbative approach can be applied to arbitrarily large perturbations, provided that enough basis states of the unperturbed system are taken into

account. It results in a simple eigenvalue equation that can be solved much faster than conventional numerical schemes for determining the RS. Under certain simplifications such as the consideration of few modes, it boils down to the so-called coupled-mode theory [99]. However, care has to be taken, because the RS cannot be used as a complete set of basis functions far outside the resonator [95], so that the considered perturbations should be in general localized in the resonator.

In the limit of a single resonant state, the resonant-state expansion yields a simple first-order perturbation theory. Thus, it is possible to describe the sensitivity of resonantly enhanced refractive-index sensors [11, 12, 26, 100, 101]. With the help of certain corrections, the first-order perturbation theory can be extended to modifications in the exterior [14, 102] as well as account for the excitation efficiency of the RS as another important quantity for optimizing a sensor [27].

The review is organized as follows: We begin with the derivation of the constitutive equation for RS, which requires to search for solutions of Maxwell's equations in the absence of sources and with outgoing boundary conditions. Afterwards, we show how the Green's dyadic can be expanded in terms of the RS. Then, we address the question of mode normalization, including a more general derivation of the analytic normalization that is valid even for nonreciprocal materials. The next subsection is devoted to orthogonality relations, followed by an overview on how to expand the near fields in terms of the RS and a discussion of the completeness of the basis of RS. Section 2 concludes with the pole expansion of the optical scattering matrix. The next section contains an overview of the different applications: resonant-state expansion, first-order perturbation theories and sensing, as well as Purcell enhancement. In the last section before the conclusion, we provide a brief introduction to related theories such as the expansion in terms of permittivity eigenmodes or propagating modes. Finally, we discuss how to use these theories to describe nonlinear optical phenomena.

2. Theory

We start with Maxwell's equations in frequency domain, which we obtain from time domain by using the Fourier transform:

$$f(\mathbf{r}; \omega) = \int dt e^{i\omega t} f(\mathbf{r}, t). \quad (1)$$

Here, ω is the angular frequency. For the sake of brevity of notations, we cast the resulting curl Maxwell's equations in a compact matrix-vector notation [91]. In Gaussian units, they read

$$\hat{\mathbb{M}}(\mathbf{r}; \omega) \mathbb{F}(\mathbf{r}; \omega) = \mathbb{J}(\mathbf{r}; \omega), \quad (2)$$

where $\hat{\mathbb{M}}(\mathbf{r}; \omega) = k\hat{\mathbb{P}} - \hat{\mathbb{D}}$ represents the so-called Maxwell operator, with $k = \omega/c$ as the vacuum wavenumber, and:

$$\hat{\mathbb{P}}(\mathbf{r}; \omega) = \begin{bmatrix} \varepsilon(\mathbf{r}; \omega) & -i\xi(\mathbf{r}; \omega) \\ i\zeta(\mathbf{r}; \omega) & \mu(\mathbf{r}; \omega) \end{bmatrix}, \quad (3)$$

$$\hat{\mathbb{D}}(\mathbf{r}) = \begin{pmatrix} 0 & \nabla \times \\ \nabla \times & 0 \end{pmatrix}. \quad (4)$$

The matrix operator $\hat{\mathbb{P}}$ contains the material parameters, namely the permittivity ε , the permeability μ , and possible bi-anisotropic contributions ξ and ζ . In general, ε , μ , ζ , and ξ are 3×3 tensors. It should be mentioned that for reciprocal materials, the material parameters obey $\xi^T = -\zeta$, $\varepsilon^T = \varepsilon$, and $\mu^T = \mu$, so that $\hat{\mathbb{P}}^T = \hat{\mathbb{P}}$, with the superscript T denoting the matrix transpose. The electric and magnetic fields \mathbf{E} and \mathbf{H} , respectively, as well as the currents \mathbf{J}_E and \mathbf{J}_H form six-dimensional supervectors:

$$\mathbb{F}(\mathbf{r}; \omega) = \begin{bmatrix} \mathbf{E}(\mathbf{r}; \omega) \\ i\mathbf{H}(\mathbf{r}; \omega) \end{bmatrix}, \quad (5)$$

$$\mathbb{J}(\mathbf{r}; \omega) = \begin{bmatrix} \mathbf{J}_E(\mathbf{r}; \omega) \\ i\mathbf{J}_H(\mathbf{r}; \omega) \end{bmatrix}. \quad (6)$$

Here, $\mathbf{J}_E(\mathbf{r}; \omega) = -4\pi i \mathbf{j}(\mathbf{r}; \omega)/c$, while the magnetic currents \mathbf{J}_H have been introduced for symmetry purposes. Note that other authors have defined various alternative formulations of a matrix-vector notation [22, 94, 95], which contain no phase factor of $\pi/2$ between electric and magnetic field.

Knowing the Green's dyadic $\hat{\mathbb{G}}$ of equation (2), which obeys the constitutive equation:

$$\hat{\mathbb{M}}(\mathbf{r}; \omega) \hat{\mathbb{G}}(\mathbf{r}, \mathbf{r}'; \omega) = \hat{\mathbb{I}} \delta(\mathbf{r} - \mathbf{r}'), \quad (7)$$

where $\hat{\mathbb{I}}$ is a six-dimensional unit matrix, we can calculate the fields for a given source as:

$$\mathbb{F}(\mathbf{r}; \omega) = \int dV' \hat{\mathbb{G}}(\mathbf{r}, \mathbf{r}'; \omega) \mathbb{J}(\mathbf{r}'; \omega). \quad (8)$$

2.1. Constitutive equation of resonant states

Consider the case of a very short excitation at time t_0 by a source $\mathbb{J}_0(\mathbf{r})\delta(t - t_0)$. In that case, the time-dependent electric fields are given by:

$$\mathcal{E}(\mathbf{r}, t) = \frac{1}{2\pi} \int d\omega e^{-i\omega(t-t_0)} \mathbf{E}(\mathbf{r}; \omega), \quad (9)$$

where \mathbf{E} is the electric field generated by the source \mathbb{J}_0 . Now assume that $\hat{\mathbb{G}}$ and, thus, \mathbf{E} has a countable number of simple poles at frequencies $\omega_n = \Omega_n - i\Gamma_n$ with $\Omega_n, \Gamma_n \in \mathbb{R}$, $\Gamma_n > 0$, and $t > t_0$. Then, the residue theorem yields for a closed surface around the negative imaginary frequency half plane that:

$$\mathcal{E}(\mathbf{r}, t) = i \sum_n e^{-i\omega_n(t-t_0)} \text{Res}[\mathbf{E}(\mathbf{r}; \omega), \omega_n]. \quad (10)$$

Hence, the time-dependent field oscillates with frequencies Ω_n while decaying in time as $\exp[-\Gamma_n(t - t_0)]$. The optical response is therefore solely determined by the fields at the complex poles. This is also illustrated in figure 2, where the transmittance of a planar slab is extended to the complex wavenumber plane. As it can be seen, the transmittance at real wavenumbers is governed by the nearest poles on the complex wavenumber plane [13].

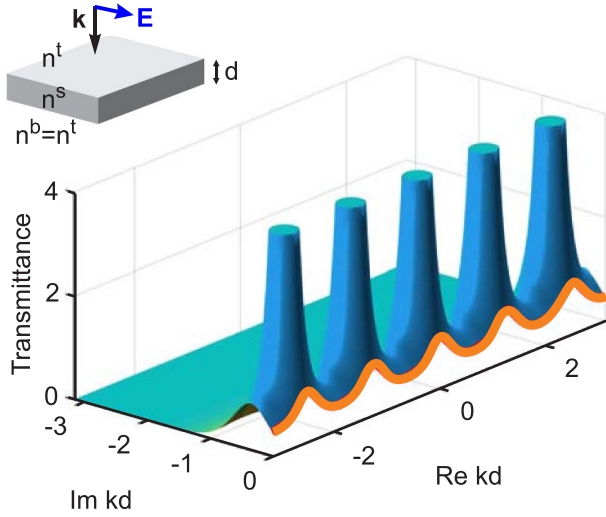


Figure 2. Analytic continuation of the transmittance of a planar dielectric slab of thickness d to the complex normalized wavenumber plane kd . The slab has a refractive index of $n = 2.5$ and is surrounded by air. The incidence direction is normal to the slab. It can be seen that the transmittance maxima at real wavenumbers are manifestations of the poles at complex wavenumbers, which can be associated with Fabry–Perot modes of different orders. Reprinted figure with permission from [13], Copyright (2018) by the American Physical Society.

Since the time-dependent field $\mathcal{E}(\mathbf{r}, t)$ must be real-valued, we infer that for every pole at a frequency ω_n , there must be another pole at $-\omega_n^*$ with residue $\text{Res}[\mathbf{E}(\mathbf{r}; \omega), -\omega_n^*] = -\text{Res}[\mathbf{E}(\mathbf{r}; \omega), \omega_n]^*$.

Equation (10) is quite descriptive. It means that a short excitation will store a finite amount of energy in the system, which will allow the resonator to oscillate at the excited resonance frequencies. While doing that, it can lose energy via different loss channels, resulting in an exponential decay of the oscillations in time with a decay rate of Γ_n . This is exactly the same process as in acoustic resonators, e.g. in a bell or guitar string that is excited by a short strike. Experimental observations of this decay are often hampered in optics by the large decay rate of typical resonances, i.e. a rather short lifetime compared to the excitation pulse. However, for long-lived resonances, the exponential decay in time can be observed, as shown by Hergert *et al* [103].

Let us now address the consequences for equation (7). If the Green's dyadic $\hat{\mathbb{G}}$ has poles at frequencies ω_n but the right-hand side of equation (7) does not depend on frequency, we can infer that the operator $\hat{\mathbb{M}}$ must have roots at these complex frequencies:

$$\hat{\mathbb{M}}(\mathbf{r}; \omega_n) \mathbb{F}_n(\mathbf{r}) = 0. \quad (11)$$

This is the constitutive equation for RS. Since the Green's dyadic yields only outgoing fields for spatial regions outside a given source \mathbb{J} , it follows that the resonant fields \mathbb{F}_n in equation (11) must possess purely outgoing boundary conditions outside the resonator. This is the reason why equation (11) can be fulfilled only for a discrete set of frequencies ω_n . Without that restriction, there exist solutions

of equation (11) for any frequency with a given incident field, which resembles the typical situation of a scattering problem in optics with a known incident field and the resulting scattered field [95].

Of course, the question is what outgoing boundary condition mean at complex frequencies. At real frequencies, we can use the Silver–Müller radiation condition [104] for isolated resonators embedded in a homogeneous and isotropic surrounding, which specify outgoing boundary conditions as:

$$\lim_{r \rightarrow \infty} \mathbf{e}_r \times \mathbf{E} = Z \mathbf{H}, \quad (12)$$

$$\lim_{r \rightarrow \infty} \mathbf{e}_r \times Z \mathbf{H} = -\mathbf{E}, \quad (13)$$

where \mathbf{e}_r is the radial unit vector and Z is the impedance of the surrounding medium. At complex frequencies, the situation is, however, more sophisticated. Most importantly, the Silver–Müller radiation condition does not hold for RS at complex frequencies [90]. Hence, it can be regarded for modal expansions in terms of RS only as the limiting case at real frequencies [95].

When considering localized sources, the definition of outgoing boundary conditions can be easily extended to complex frequencies: If a source \mathbb{J} is completely localized in a certain volume, then the fields generated by this source are purely outgoing outside that volume. The problem is that equation (11) does not contain any sources. Still, it is possible to test the boundary conditions of solutions of equation (11) by introducing a localized source that vanishes in the limit $\omega \rightarrow \omega_n$, i.e. $\mathbb{J} \propto \mathcal{O}(\omega - \omega_n)$. The fields \mathbb{F} generated by this source then have to obey $\mathbb{F} \rightarrow \mathbb{F}_n$ for $\omega \rightarrow \omega_n$. Note that this approach is also used for deriving the analytic normalization in the next section. Of course, one needs to clarify, where possible sources are located in this case. For this purpose, we separate our system into a background system with a trivial material distribution $\hat{\mathbb{P}}_{\text{BG}}$ that should be free of RS, and a localized non-trivial variation $\Delta \hat{\mathbb{P}}$ that constitutes the resonator:

$$\hat{\mathbb{P}}(\mathbf{r}; \omega) = \hat{\mathbb{P}}_{\text{BG}}(\mathbf{r}; \omega) + \Delta \hat{\mathbb{P}}(\mathbf{r}; \omega). \quad (14)$$

Possible test sources for outgoing boundary conditions should be located in regions with $\Delta \hat{\mathbb{P}} \neq 0$.

Still, there can be some ambiguity about the optimal set of RS. For instance, in planar periodic structures, Rayleigh–Wood anomalies [75–77] arise in the spectra. They occur spectrally, whenever a plane wave in the super- or substrate changes between propagating and decaying perpendicular to the planar system. In that case, the wavevector component perpendicular to the slab, which we denote here as k_z , approaches zero. As discussed later, this yields cuts in the complex frequency plane for the expansion of the Green's dyadic [17, 105]. The exact path of these cuts is not unique [83], but can be chosen in dependence of the selection of Riemann sheets in the square root function that relates k_z with the vacuum wavenumber k via:

$$k_z = \pm \sqrt{n^2 k^2 - \mathbf{k}_{\parallel}^2}, \quad (15)$$

where n is the refractive index in the super- or substrate and \mathbf{k}_{\parallel} is the projection of the wavevector parallel to the planar structure. A common selection for the Riemann sheet with outgoing plane waves, i.e. when to use the positive or negative sign in equation (15), is to warrant $\text{Re}(k_z) + \text{Im}(k_z) > 0$, but other definitions may be better suited. In some cases, it even turns out that a description of the optical response in terms of complex propagation constants k_z is favorable over an analytic continuation to complex frequencies [17, 105]. In that case, it is then possible to account for modes on both Riemann sheets simultaneously, while the related cut contribution is removed.

Finally, let us briefly address the question on how to obtain solutions of equation (11). In the cases of planar slabs, spherical particles, or infinitely long cylinders, we can derive the RS and their complex resonance frequencies by reducing Maxwell's equations to a transcendental equation that can be solved exactly up to machine precision. In very specific cases such as planar slabs consisting of homogeneous and isotropic non-dispersive materials, it is even possible to write down closed expressions for the resonance frequencies and fields [17, 94, 106]. In general, however, numerical methods are required to determine solutions of equation (11). An overview and benchmark of common methods can be found in [107]. Alternatively, the RS of a complex system can be calculated from simpler systems with known analytic solutions via the resonant-state expansion [1, 91], see also section 3.1.

2.2. Pole expansion of the Green's dyadic

We derive now an expansion of the Green's dyadic in terms of poles and residues that is based on the Mittag-Leffler theorem [1, 91]. Let us briefly summarize this theorem: if $f(z)$ is a complex function that is analytic except for a countable number of poles a_n with residues b_n and the asymptotic behavior $\lim_{z \rightarrow \infty} f(z)/z^p = 0$, it can be expanded as [106, 108]:

$$f(z) = f_p(z) + \sum_n \frac{b_n}{(z - a_n)}, \quad (16)$$

where $f_0 = 0$ and

$$f_p(z) = \sum_{m=0}^{p-1} \left[\frac{f^{(m)}(0)}{m!} + \sum_n \frac{b_n}{a_n^{m+1}} \right] z^m. \quad (17)$$

That means that for any order p , we obtain a pole contribution of the form $\sum_n b_n/(z - a_n)$, accompanied for $p > 0$ by a polynomial of order $p - 1$. Let us consider a source term $\mathbb{J}_n = (\omega - \omega_n) \mathbb{S}_n / c$ with a localized source \mathbb{S}_n that generates a field \mathbb{F} and vanishes at the resonance frequency ω_n :

$$\hat{\mathbb{M}}(\mathbf{r}; \omega) \mathbb{F}(\mathbf{r}; \omega) = \frac{\omega - \omega_n}{c} \mathbb{S}_n(\mathbf{r}). \quad (18)$$

Since $\lim_{\omega \rightarrow \omega_n} \mathbb{F} = \mathbb{F}_n$, it is possible to show using equation (8) that if the Green's dyadic is analytic and

$\lim_{\omega \rightarrow \infty} \hat{\mathbb{G}} = 0$ except for a countable number of poles, it must be of the following form [12, 91]:

$$\hat{\mathbb{G}}(\mathbf{r}, \mathbf{r}'; \omega) = c \sum_n \frac{\mathbb{F}_n(\mathbf{r}) \otimes \mathbb{X}_n(\mathbf{r}')}{\omega - \omega_n}. \quad (19)$$

Yet, this expression contains unknown fields \mathbb{X}_n that we will determine in the following.

Inspired by the generalization of the reciprocity theorem [109], we consider now the transposed system:

$$\hat{\mathbb{M}}^\ddagger(\mathbf{r}; \omega) \mathbb{F}^\ddagger(\mathbf{r}; \omega) = \mathbb{J}^\ddagger(\mathbf{r}; \omega), \quad (20)$$

which differs from the original system in the sense that the material operator $\hat{\mathbb{P}}$ is replaced by its matrix-transposed counterpart $\hat{\mathbb{P}}^\ddagger$ so that the Maxwell operator is modified to $\hat{\mathbb{M}}^\ddagger = k \hat{\mathbb{P}}^\ddagger - \hat{\mathbb{D}}$. The superscript \ddagger is used to label quantities in this transposed system. It should be noted that $\mathbb{J}^\ddagger = \mathbb{J}$ does not imply $\mathbb{F}^\ddagger = \mathbb{F}$, except for reciprocal systems with $\hat{\mathbb{P}}^\ddagger = \hat{\mathbb{P}}$. The Green's dyadic of $\hat{\mathbb{M}}^\ddagger$ therefore differs in general from $\hat{\mathbb{G}}$ and will be denoted by $\hat{\mathbb{G}}^\ddagger$.

In order to obtain further relations for the transposed fields \mathbb{F}^\ddagger , we assume arbitrary sources \mathbb{J}_1 and \mathbb{J}_2^\ddagger that are extended over a finite region in space and generate fields \mathbb{F}_1 and \mathbb{F}_2^\ddagger . Then, we multiply equations (2) and (20) from the left with \mathbb{F}_2^\ddagger and \mathbb{F}_1 , respectively, and subtract the results, which yields:

$$\mathbb{F}_1 \cdot \hat{\mathbb{D}} \mathbb{F}_2^\ddagger - \mathbb{F}_2^\ddagger \cdot \hat{\mathbb{D}} \mathbb{F}_1 = \mathbb{F}_2^\ddagger \cdot \mathbb{J}_1 - \mathbb{F}_1 \cdot \mathbb{J}_2^\ddagger. \quad (21)$$

Integrating this equation over a finite volume V and using the identity [13]

$$\int_V dV (\mathbb{F}_1 \cdot \hat{\mathbb{D}} \mathbb{F}_2^\ddagger - \mathbb{F}_2^\ddagger \cdot \hat{\mathbb{D}} \mathbb{F}_1) = i \oint_{\partial V} d\mathbf{S} \cdot (\mathbf{E}_2^\ddagger \times \mathbf{H}_1 - \mathbf{E}_1 \times \mathbf{H}_2^\ddagger) \quad (22)$$

results in

$$i \oint_{\partial V} d\mathbf{S} \cdot (\mathbf{E}_2^\ddagger \times \mathbf{H}_1 - \mathbf{E}_1 \times \mathbf{H}_2^\ddagger) = \int_V dV (\mathbb{F}_2^\ddagger \cdot \mathbb{J}_1 - \mathbb{F}_1 \cdot \mathbb{J}_2^\ddagger). \quad (23)$$

In his tutorial [95], Kristensen derived a suitable bi-orthogonal basis by the condition that a similar surface integral as that on the left-hand side of equation (23) must vanish. We follow this idea, but approach it from a different direction. More specifically, we consider here generalized reciprocity relations. In the simple case of reciprocal materials, it can be shown that [11, 109]:

$$\hat{\mathbb{G}}^T(\mathbf{r}, \mathbf{r}'; \omega) = \hat{\mathbb{G}}(\mathbf{r}', \mathbf{r}; \omega). \quad (24)$$

This relation can be generalized when reversing all external bias. For instance, when breaking reciprocity by a static magnetic field, this requires reversing the direction of the static magnetic field. Using the Onsager–Casimir relation that is based on the work of Onsager and Casimir [110–112], it then follows [109]:

$$\hat{\mathbb{G}}^\ddagger(\mathbf{r}, \mathbf{r}'; \omega) = \hat{\mathbb{G}}^T(\mathbf{r}', \mathbf{r}; \omega). \quad (25)$$

Expressing the fields \mathbb{F}_1 and \mathbb{F}_2^\dagger on the right-hand side of equation (23) via equation (8) and its transposed counterpart, respectively, we obtain from equation (25) that the right-hand side of equation (23) vanishes:

$$\int_V dV \int_V dV' [(\hat{\mathbb{G}}^\dagger \mathbb{J}_2^\dagger) \cdot \mathbb{J}_1 - \mathbb{J}_2^\dagger \cdot \hat{\mathbb{G}} \mathbb{J}_1] = 0. \quad (26)$$

Hence, the left-hand side of equation (23) must equal zero, too:

$$\oint_{\partial V} d\mathbf{S} \cdot (\mathbf{E}_2^\dagger \times \mathbf{H}_1 - \mathbf{E}_1 \times \mathbf{H}_2^\dagger) = 0. \quad (27)$$

This is a necessary condition for pairs of fields that obey the prerequisites of the Onsager–Casimir relation [109] and are generated by sources that are completely localized inside the volume V . Due to the latter condition, these fields are inherently outgoing on ∂V . Often, this condition is trivially fulfilled. However, in some cases, one needs to be more careful in reversing all external bias. For instance, for planar bi-periodic systems, one can select a phase factor $\exp(i\mathbf{k}_\parallel \cdot \mathbf{r})$ for the fields, where \mathbf{k}_\parallel is a vector in the plane with periodic boundary conditions [12]. This phase factor is preserved within the whole system. Reversing the external bias means going from \mathbf{k}_\parallel to $-\mathbf{k}_\parallel$ for the transposed fields \mathbb{F}^\dagger . In [13, 84, 102, 106, 113, 114], this form of reversing the external bias is called ‘reciprocal conjugation’ and denoted by a superscript R, because the considered systems are composed of purely reciprocal materials.

It should be noted that equation (27) also holds in the case that both sources \mathbb{J}_1 and \mathbb{J}_2^\dagger are outside the volume V , in which case \mathbb{F}_1 and \mathbb{F}_2^\dagger are pairs of incoming fields. Based on these arguments, the only possibility for the left-hand side of equation (23) to be nonzero when reversing all external bias between \mathbb{F}_1 and \mathbb{F}_2^\dagger is that we consider pairs of incoming and outgoing fields, which is used in [13] to construct the pole expansion of the scattering matrix. In that case, we select appropriate basis sets to ensure that the left-hand side of equation (23) is non-vanishing for pairs of incoming and outgoing fields.

Finally, we can infer from equation (25) that $\hat{\mathbb{G}}$ and $\hat{\mathbb{G}}^\dagger$ have the same poles, i.e. the operators $\hat{\mathbb{M}}$ and $\hat{\mathbb{M}}^\dagger$ possess the same spectrum. The constitutive equation for the transposed RS is:

$$\hat{\mathbb{M}}^\dagger(\mathbf{r}; \omega_n) \mathbb{F}_n^\dagger(\mathbf{r}) = 0. \quad (28)$$

Note that in general $\mathbb{F}_n \neq \mathbb{F}_n^\dagger$. However, we may follow the same steps as for deriving equation (19) to obtain the pole expansion of $\hat{\mathbb{G}}^\dagger$, where \mathbb{F}_n and \mathbb{X}_n are replaced by \mathbb{F}_n^\dagger and an unknown field \mathbb{X}_n^\dagger . Then, using equation (25), we obtain the analytic pole expansion of the Green’s dyadic:

$$\hat{\mathbb{G}}(\mathbf{r}, \mathbf{r}'; \omega) = c \sum_n \frac{\mathbb{F}_n(\mathbf{r}) \otimes \mathbb{F}_n^\dagger(\mathbf{r}')}{\omega - \omega_n}. \quad (29)$$

An alternative way of deriving this relation is to expand the operator $\hat{\mathbb{M}}$ in a suitable basis, in which equation (11) yields

a nonlinear matrix-eigenvalue equation. In numerical calculations, this is done via a discretization of the computational domain, resulting in a finite-sized nonlinear eigenvalue problem [94, 115–117]. Then, using Keldysh theorem [118, 119], the expansion of the resolvent is straight-forward [115], with the representation of \mathbb{F}_n^\dagger being a left eigenvector of the nonlinear eigenvalue equation.

At the end of this subsection, let us use the pole expansion of the Green’s dyadic to derive some further relations, which are of general usefulness. By inserting equation (29) into equation (7), we obtain the closure relation [91]:

$$\sum_n \frac{\omega \hat{\mathbb{P}}(\mathbf{r}; \omega) - \omega_n \hat{\mathbb{P}}(\mathbf{r}; \omega_n)}{\omega - \omega_n} \mathbb{F}_n(\mathbf{r}) \otimes \mathbb{F}_n^\dagger(\mathbf{r}') = \hat{\mathbb{I}} \delta(\mathbf{r} - \mathbf{r}'). \quad (30)$$

Assuming material distributions of the form:

$$\hat{\mathbb{P}}(\mathbf{r}; \omega) = \hat{\mathbb{P}}(\mathbf{r}) + \sum_j \frac{\hat{\mathbb{Q}}_j}{\omega - \Omega_j}, \quad (31)$$

where Ω_j are complex poles of the material response with residues $\hat{\mathbb{Q}}_j$ [120], it is furthermore shown in [91] how to derive the following sum rules:

$$\hat{\mathbb{Q}}_j(\mathbf{r}) \sum_n \frac{\mathbb{F}_n(\mathbf{r}) \otimes \mathbb{F}_n^\dagger(\mathbf{r}')}{\omega_n - \Omega_j} = 0. \quad (32)$$

Other forms of sum rules can be found in [7, 96], and a combination of the sum and closure relation yields [91]:

$$\sum_n \hat{\mathbb{P}}(\mathbf{r}; \omega_n) \mathbb{F}_n(\mathbf{r}) \otimes \mathbb{F}_n^\dagger(\mathbf{r}') = \hat{\mathbb{I}} \delta(\mathbf{r} - \mathbf{r}'). \quad (33)$$

The implications of the sum rules and closure relations are discussed later in the context of the completeness of the basis of RS. Furthermore, the sum rules can be used to obtain the connection between different formulations of the resonant expansion [106].

2.3. Normalization of resonant states

Equation (11) specifies the resonant field distributions \mathbb{F}_n only up to a complex scalar factor. While we can infer from equation (10) that it should be possible to decompose arbitrary fields into their resonant contributions, i.e. to assume that the RS constitute a complete basis set, such an expansion requires to fix the arbitrariness of the complex scalar factor and to normalize the resonant field distributions uniquely.

For bound eigenstates ψ_n in quantum mechanics and lossless waveguides, it is possible to derive a simple orthogonality relation as:

$$\int dV \psi_n^* \psi_m = \delta_{nm}, \quad (34)$$

which contains an integral over the entire space and allows for normalizing the wave functions ψ_n for a general expansion in terms of these eigenfunctions. For RS, the situation is not

as trivial. For instance, RS in spherical particles satisfy outgoing fields that scale as $\exp(i\omega_n r/c)/r$ for large distances to the particles. If $\omega_n = \Omega_n - i\Gamma_n$ with $\Gamma_n > 0$ in order to yield a solution that is decaying exponentially in time, its spatial fields scale as $\exp(i\Omega_n r/c + \Gamma_n r/c)/r$, i.e. they grow exponentially with r . This diverging behavior is common to all RS that lose energy via radiation to the surrounding. Hence, a normalization similar to equation (34) is not possible for those RS, because the integral over the entire space will diverge.

Of course, one may ask if the growing character of resonant field distributions is unphysical. However, as indicated in the introduction, there is a simple physical explanation: the fields further away from the resonator have left the resonator at an earlier time at which more energy had been stored in it. The energy is then lost via radiative and nonradiative processes. The radiative processes carry energy away with the speed of light, which is fully consistent with causality [121]. The divergent nature of the RS can be thus interpreted as if an infinite amount of energy had been stored in the resonator at $t_0 \rightarrow -\infty$ and is now distributed over all space.

In early works related to first-order perturbation theories [100] and Purcell factors [122] of RS in open cavities, the divergence of RS was either ignored or overlooked, and the integration over the fields was restricted to a finite volume. While this may work out reasonably well for some cases, it has been noted already by Koenderink [123] that the divergence of such integrals cannot provide accurate results in general. However, the simplicity of the incorrect theory and its good agreement with many expectations and observations has prevented the derivation of a more advanced theory for nanophotonics for more than a decade.

Solutions for a correct normalization of growing fields were available—either in quantum mechanics [79, 80, 124] or waveguide theory [81, 82]. Most common is to regularize the functions [79] or to make the system finite by a complex coordinate transformation [81, 82]. It is the merit of Sauvan and Lalanne to reinvent the latter method for applications in nanophotonics and to formalize it in the framework of the theory of perfectly-matched layers [3, 94]: an infinite system can be mapped via a complex-valued coordinate transformation to an equivalent finite system, in which there is no divergence of fields at the boundaries if all parameters are chosen appropriately. This is equivalent to surrounding a given geometry by perfectly-matched layers [125], which is therefore the most common implementation of this normalization in numerical calculations. Mathematically, the resulting normalization can be written for $\zeta = \xi = 0$ as:

$$\int_{\tilde{V}} dV \left[\tilde{\mathbf{E}}_n \cdot \frac{\partial \omega \tilde{\epsilon}}{\partial \omega} \Big|_{\omega_n} \tilde{\mathbf{E}}_n - \tilde{\mathbf{H}}_n \cdot \frac{\partial \omega \tilde{\mu}}{\partial \omega} \Big|_{\omega_n} \tilde{\mathbf{H}}_n \right] = 1, \quad (35)$$

where \tilde{V} denotes a finite volume including the region of the perfectly-matched layers. While this approach is rather versatile, it is a bit problematic that the important fact that \tilde{V} is not the entire infinite space often just shows up as a footnote. Hence, equation (35) makes the impression of a divergent

integral. Moreover, the fields inside the region of perfectly-matched layers are related to the original fields in real space only by the corresponding complex coordinate transformation, and the original permittivity and permeability have to be replaced there by those artificial quantities of the perfectly-matched layers, see supplementary material of [3]. That is why we have added a tilde on top of the fields and material parameters in equation (35). Finally, the selection of appropriate parameters for the perfectly-matched layers can be rather delicate in some cases. Therefore, it has to be carefully checked that equation (35) has converged.

Alternatively, analytic approaches for the normalization can be formulated, in which the divergent integrals are considered in a distribution sense [126] or a surface contribution is derived to compensate for the divergence of the volume integral, see [91] and references therein. Here, we will focus on the latter approach, which is based on assigning the correct weight to the residues in the Mittag-Leffler expansion of the Green's dyadic provided in equation (29).

So far, neither \mathbb{F}_n nor \mathbb{F}_n^\dagger are defined uniquely by equation (11) and its transposed counterpart equation (28). Selecting the source term \mathbb{S}_n in equation (18) such that $\int_V dV \mathbb{F}_n^\dagger \cdot \mathbb{S}_n = 1$, and following the derivation steps in [91] and references therein, we arrive at the normalization condition:

$$1 = V_n + S_n, \quad (36)$$

where

$$V_n = \int_V dV \mathbb{F}_n^\dagger \cdot (\omega \hat{\mathbb{P}})' \mathbb{F}_n, \quad (37)$$

$$S_n = ic \oint_{\partial V} d\mathbf{S} (\mathbf{E}_n^\dagger \times \mathbf{H}_n' - \mathbf{E}_n' \times \mathbf{H}_n^\dagger), \quad (38)$$

and the prime denotes the derivative with respect to ω at ω_n . Note that equation (37) resembles the left-hand side of equation (35) for $\zeta = \xi = 0$, except for V being an arbitrary volume surrounding the scattering geometry without the need for any perfectly-matched layers. In figure 3, one can see that the normalization as the sum of surface and volume term is actually independent of the volume of integration, which is highly beneficial in complex systems, where a larger computational domain increases the calculation time significantly. The price to pay is that one needs to evaluate a field derivative in the surface term in equation (38).

At a first glance, it seems counterintuitive that \mathbb{F}_n as the eigensolution of equation (11) has any frequency dependence for calculating the field derivative. In fact, one needs to consider equation (18) in the limit $\omega \rightarrow \omega_n$. Applying equation (8) in equation (18) and inserting the Green's dyadic expansion from equation (29), we obtain:

$$\mathbb{F}(\mathbf{r}; \omega) = \sum_m \frac{\omega - \omega_n}{\omega - \omega_m} \mathbb{F}_m(\mathbf{r}) \int dV' \mathbb{F}_m^\dagger(\mathbf{r}') \cdot \mathbb{S}_n(\mathbf{r}'). \quad (39)$$

This is the starting point for defining the derivative \mathbb{F}_n' . However, some additional steps are necessary to obtain the final

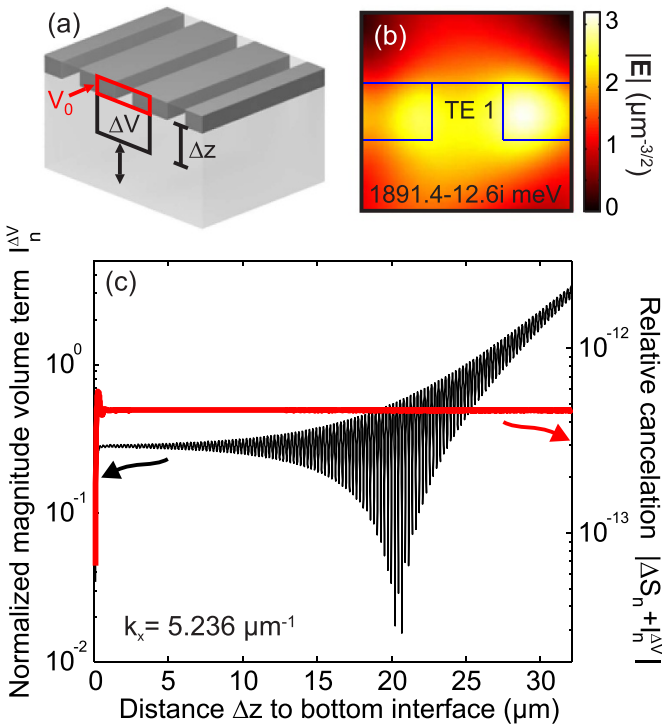


Figure 3. Independence of the analytic normalization on the volume of integration demonstrated for a one-dimensional photonic crystal slab. The geometry is depicted in (a), with ΔV being the extension of the volume of normalization into the substrate and V_0 as the minimum volume of normalization. The electric-field magnitude of a fundamental transverse-electric (TE) mode at an in-plane momentum of $k_x = 5.236 \mu\text{m}^{-1}$ is displayed in (b). In panel (c), we can see the dependence of the volume term (black solid line) of this mode on the volume of normalization. It is evident that the magnitude of the volume term grows exponentially. However, the sum of the change of volume and surface term (red solid line) remains constant within the accuracy of our numerical method [12, 127, 128]. Reprinted figure with permission from [12], Copyright (2017) by the American Physical Society.

result. We may be tempted to consider equation (39) as an analytic continuation of \mathbb{F}_n to the complex frequency plane and simply calculate \mathbb{F}'_n via the derivative of \mathbb{F} with respect to ω at ω_n . However, this results in an expression that depends on all RS and the specific form of \mathbb{S}_n . Moreover, as discussed later, it is questionable if such an expansion is valid everywhere in the external surrounding.

Instead, we have to show that we can define \mathbb{F}'_n such that it does not depend on other RS and the precise form of \mathbb{S}_n . We are deriving here a more general proof than in [11, 12], which starts with the separation of equation (18) into background material $\hat{\mathbb{P}}_{\text{BG}}$ and resonator contribution $\Delta\hat{\mathbb{P}}$:

$$\hat{\mathbb{M}}_{\text{BG}}\mathbb{F} = -\frac{\omega}{c}\Delta\hat{\mathbb{P}}\mathbb{F} + \frac{\omega - \omega_n}{c}\mathbb{S}_n. \quad (40)$$

Here, we have introduced the Maxwell operator of the background system as:

$$\hat{\mathbb{M}}_{\text{BG}} = \frac{\omega}{c}\hat{\mathbb{P}}_{\text{BG}} - \hat{\mathbb{D}}. \quad (41)$$

Let us assume that we know the Green's dyadic $\hat{\mathbb{G}}_0$ of the background system, which allows us to reformulate equation (40) via equation (8) as:

$$\mathbb{F} = \int_V dV \hat{\mathbb{G}}_0 \left(-\frac{\omega}{c}\Delta\hat{\mathbb{P}}\mathbb{F} + \frac{\omega - \omega_n}{c}\mathbb{S}_n \right). \quad (42)$$

If $\mathbb{S}_n = 0$, this formulation is equivalent to the regularized resonant fields in [4].

Expanding \mathbb{F} , $\hat{\mathbb{G}}_0$, and $\omega\Delta\hat{\mathbb{P}}$ into Taylor series around ω_n and sorting in powers of $\omega - \omega_n$ yields in the zeroth order equation (11), while the first-order correction is:

$$\begin{aligned} \mathbb{F}' = & -\frac{\omega_n}{c} \int_V dV \hat{\mathbb{G}}_0' \Delta\hat{\mathbb{P}}(\omega_n)\mathbb{F}_n \\ & + \frac{1}{c} \int_V dV \hat{\mathbb{G}}_0 \left[\mathbb{S}_n - (\omega\Delta\hat{\mathbb{P}})' \mathbb{F}_n - \omega_n \Delta\hat{\mathbb{P}}(\omega_n)\mathbb{F}' \right]. \end{aligned} \quad (43)$$

The second line contains only sources located inside the resonator, so that it yields purely outgoing fields outside the resonator. Hence, we infer from the condition given by equation (27) that the fields generated by this source do not contribute to the surface integral in equation (38). The first line, however, contains the derivative $\hat{\mathbb{G}}_0'$ instead of the Green's dyadic, so that we must assume that this results in a nonvanishing contribution to equation (38). Therefore, we may define \mathbb{F}'_n via:

$$\mathbb{F}'_n = -\frac{\omega_n}{c} \int_V dV \hat{\mathbb{G}}_0' \Delta\hat{\mathbb{P}}(\omega_n)\mathbb{F}_n, \quad (44)$$

which is solely given by the underlying differential equation and the corresponding resonant field distribution \mathbb{F}_n .

Of course, it is not very practical to calculate \mathbb{F}'_n via equation (44), because we need to know $\hat{\mathbb{G}}_0$. However, the above considerations at least tell us that \mathbb{F}'_n does not depend on the selection of the source \mathbb{S}_n in the derivation of the normalization. Hence, \mathbb{F}'_n is a quantity that is uniquely defined by the resonant state.

In practical calculations, we need to find suitable ways to derive \mathbb{F}'_n in the exterior surrounding of the resonator geometry. If the surrounding is rather trivial with a known set of basis functions, any field distribution generated by sources inside the resonator can be expanded in terms of the subset of outgoing basis functions $\mathbb{O}_{\mathbf{N}}$ of the surrounding system [13]. Here, \mathbf{N} is a vector that summarizes all labels to distinguish the outgoing basis functions. Thus, equation (39) can be written as:

$$\mathbb{F}(\mathbf{r}; \omega) = \sum_m \frac{\omega - \omega_n}{\omega - \omega_m} \sum_{\mathbf{N}} \alpha_{\mathbf{N}}^{(m)}(\omega) \mathbb{O}_{\mathbf{N}}(\mathbf{r}; \omega) I_{m\mathbf{N}}, \quad (45)$$

where $I_{m\mathbf{N}} = \int dV V_m^\dagger(\mathbf{r}') \cdot \mathbb{S}_n(\mathbf{r}')$ with $I_{m\mathbf{N}} = 1$ by definition, and $\alpha_{\mathbf{N}}^{(m)}$ is the frequency-dependent expansion coefficient of the resonant state with field \mathbb{F}_m .

If we now differentiate equation (45) with respect to ω at ω_n , we already know that all other modes with index $m \neq n$

must not contribute to \mathbb{F}'_n . The only question is about the contribution of the terms $(\alpha_N^{(n)})' \mathbb{O}_N$, where the prime denotes the frequency derivative of the expansion coefficient at frequency ω_n . Since this part is proportional to \mathbb{O}_N at ω_n , we obtain from equation (27) that it must not contribute to equation (38) either. Hence, we can calculate \mathbb{F}'_n in equation (38) via:

$$\mathbb{F}'_n(\mathbf{r}) = \sum_N \alpha_N^{(n)}(\omega_n) \mathbb{O}'_N(\mathbf{r}), \quad (46)$$

where \mathbb{O}'_N is the frequency derivative of \mathbb{O}_N at ω_n . This approach for calculating \mathbb{F}'_n has been used, e.g. for normalizing RS in planar periodic system [11, 12]. For isolated nanostructures in a homogeneous and isotropic surrounding, it is possible to convert the frequency derivative into a spatial derivative [1, 7, 91], which simplifies the calculation of \mathbb{F}'_n significantly.

It should be mentioned that in earlier works on analytic normalizations with surface terms, the starting point was the wave equation instead of the curl Maxwell's equations [1, 5–7, 11, 12, 17]. It has been shown that for nonmagnetic materials, these normalizations are equivalent to equation (36), except for an artificial factor of $\sqrt{2}$ [91]. However, they cannot be used for magnetic, bi-isotropic, and bi-anisotropic materials.

Comparing the normalization via perfectly-matched layers with the analytic normalization, the advantage of the perfectly-matched layers is that this approach can be used for any sort of resonator geometry. However, care has to be taken regarding the proper definition of the perfectly-matched layers. If they do not suppress back-reflection sufficiently or their discretization is not selected appropriately, the normalization via perfectly-matched layers will provide inaccurate results. Furthermore, as noted above, in systems such as planar slabs, the definition of incoming and outgoing fields may be not straightforward on the complex frequency plane in the vicinity of Rayleigh–Wood anomalies. It may then happen that certain RS cannot be found numerically. Finally, not all numerical methods include perfectly-matched layers. In the case of the analytic normalization, the advantage is that we can obtain fully analytic equations in some cases such as slabs [17] or spheres [5]. Furthermore, it is possible to restrict the computational domain to a minimal volume surrounding the resonator. The main requirement is that the fields are calculated accurately enough at the surface and in the interior. The disadvantage is that there is only a limited number of systems with known surface integrals. Most importantly, the practically relevant case of a single resonator on top of a substrate is yet not solved analytically.

It should be mentioned that an alternative numerical normalization procedure is described in [88, 129]. In this approach, the system is driven by a source that oscillates at a complex frequency in the vicinity of the pole at ω_n . Then, it is assumed that the resulting field distribution resembles the correctly normalized resonant state \mathbb{F}_n multiplied by some proportionality factor, which can be deduced easily. In some sense, this can be considered as a numerical variant of assigning the correct weight to the residues of the Green's dyadic.

2.4. Orthogonality relation

When considering equation (11) for a mode with index n and equation (28) for a mode with index m , we may multiply equation (11) with \mathbb{F}_m^\dagger and equation (28) with \mathbb{F}_n to obtain:

$$\mathbb{F}_m^\dagger \cdot \left[\frac{\omega_n}{c} \hat{\mathbb{P}}(\omega_n) - \frac{\omega_m}{c} \hat{\mathbb{P}}(\omega_m) \right] \mathbb{F}_n - \mathbb{F}_m^\dagger \cdot \hat{\mathbb{D}} \mathbb{F}_n + \mathbb{F}_n \cdot \hat{\mathbb{D}} \mathbb{F}_m^\dagger = 0. \quad (47)$$

Integrating over a volume V and using the vector identities in equation (22) results in the following orthogonality relation:

$$\int_V dV \mathbb{F}_m^\dagger \cdot \left[\omega_n \hat{\mathbb{P}}(\omega_n) - \omega_m \hat{\mathbb{P}}(\omega_m) \right] \mathbb{F}_n - ic \oint_{\partial V} d\mathbf{S} \cdot (\mathbf{E}_m^\dagger \times \mathbf{H}_n - \mathbf{E}_n \times \mathbf{H}_m^\dagger) = 0. \quad (48)$$

Similar expressions are given in [5] for non-dispersive and non-magnetic systems. In the case that we enclose the system by perfectly-matched layers, one may argue that the surface integral vanishes at the outermost interfaces of the perfectly-matched layers, resulting in the following orthogonality relation [94]:

$$\int_{\tilde{V}} dV \tilde{\mathbb{F}}_m^\dagger \cdot \left[\omega_n \tilde{\mathbb{P}}(\omega_n) - \omega_m \tilde{\mathbb{P}}(\omega_m) \right] \tilde{\mathbb{F}}_n = 0. \quad (49)$$

2.5. Near-field expansion

Using equation (29) in equation (8), it is possible to construct the Green's dyadic, and, thus, the fields generated by an internal source:

$$\mathbb{F}(\mathbf{r}; \omega) = c \sum_n \frac{\mathbb{F}_n(\mathbf{r})}{\omega - \omega_n} \int dV' \mathbb{F}_n^\dagger(\mathbf{r}') \cdot \mathbb{J}(\mathbf{r}'; \omega). \quad (50)$$

This yields a suitable near-field expansion for local sources that can be used in many practical applications [3, 7, 94]. Often, one is, however, not interested in the field that is generated by a local source \mathbb{J} , but in the scattered field that is generated by a given incident field. Following the derivations of [106], we now derive an expression for this scattered field.

Let us consider a region in space that is free of sources, i.e. the right-hand side of equation (2) is zero. In that case, the electromagnetic fields usually consist of incoming and outgoing parts. As described in [13, 94], we first separate the total system into a background system with material distribution $\hat{\mathbb{P}}_{\text{BG}}$ and a local material change $\Delta \hat{\mathbb{P}} = \hat{\mathbb{P}} - \hat{\mathbb{P}}_{\text{BG}}$ for the resonator, see equation (14). Then an arbitrary incoming field \mathbb{I}_{BG} may be regarded as the incoming part of a background field $\mathbb{F}_{\text{BG}} = \mathbb{I}_{\text{BG}} + \mathbb{O}_{\text{BG}}$, where \mathbb{O}_{BG} is the corresponding outgoing field. The background field \mathbb{F}_{BG} is a solution of the following Maxwell's equations:

$$\hat{\mathbb{M}}_{\text{BG}}(\mathbf{r}; \omega) \mathbb{F}_{\text{BG}}(\mathbf{r}; \omega) = 0. \quad (51)$$

Here, $\hat{\mathbb{M}}_{\text{BG}}$ is the Maxwell operator of the background system, see equation (41). Thus, the total field supervector can be expressed as a superposition of the background and a scattered field as $\mathbb{F}_{\text{tot}} = \mathbb{F}_{\text{BG}} + \mathbb{F}_{\text{scat}}$. Although it is common to consider homogeneous and isotropic background material distributions $\hat{\mathbb{P}}_{\text{BG}}$, it is as well possible to introduce more complex background systems such as planar interfaces between two materials to account, e.g. for the presence of substrates. After some algebra, we obtain [13, 94]:

$$\hat{\mathbb{M}}(\mathbf{r}; \omega) \mathbb{F}_{\text{scat}}(\mathbf{r}; \omega) = -\frac{\omega}{c} \Delta \hat{\mathbb{P}}(\mathbf{r}; \omega) \mathbb{F}_{\text{BG}}(\mathbf{r}; \omega). \quad (52)$$

The right-hand side can be interpreted as an internal source for the scattered field, which allows us to construct the total field via equation (50) as [106]:

$$\mathbb{F}_{\text{tot}}(\mathbf{r}; \omega) = \mathbb{F}_{\text{BG}}(\mathbf{r}; \omega) - \sum_n \frac{I_n(\omega)}{\omega - \omega_n} \mathbb{F}_n(\mathbf{r}), \quad (53)$$

where we have introduced the overlap integral I_n as:

$$I_n(\omega) = \omega \int dV \mathbb{F}_n^\dagger(\mathbf{r}) \cdot \Delta \hat{\mathbb{P}}(\mathbf{r}; \omega) \mathbb{F}_{\text{BG}}(\mathbf{r}; \omega). \quad (54)$$

The pole expansion of the total field given by equation (53) is broadly used as a semi-analytical method to expand the near fields for a given resonator system [13, 88, 94]. However, it has been noted that such an expansion is not unique [94, 106, 117, 130, 131]. For instance, several formulations are benchmarked numerically for Lorentz-dispersive materials [131], and a whole family of possible expansions with different frequency-dependent weight functions is discussed in [117]. Unger and coworkers suggest an independent expansion of electric and magnetic fields [130], which provides more degrees of freedom and can be very efficiently applied for certain geometries and materials with $\zeta = \xi = 0$.

While equation (52) and most other formulations contain weight functions of the poles that depend on frequency, the work in reference [106] provides an alternative formulation with constant weight functions. The idea is to consider equation (52) as a function that is analytic except for a countable number of poles and to apply the Mittag-Leffler theorem once more. Care has to be taken, however, because the asymptotic behavior is usually more sophisticated than that of the Green's dyadic. This means that one has to check if the prerequisites for the Mittag-Leffler theorem are fulfilled. Often, higher-order versions of the Mittag-Leffler theorem have to be applied, i.e. $p > 0$ in equation (16). If the background field is free of poles, such as in the case of a homogeneous and isotropic background material, the p th-order Mittag-Leffler expansion of the total field yields:

$$\mathbb{F}_{\text{tot}}(\mathbf{r}; \omega) = \mathbb{F}_p(\mathbf{r}; \omega) - \sum_n \frac{I_n(\omega_n)}{(\omega - \omega_n)^p} \mathbb{F}_n(\mathbf{r}), \quad (55)$$

where $\mathbb{F}_0 = 0$, while \mathbb{F}_p is a polynomial of order $p - 1$:

$$\mathbb{F}_p(\mathbf{r}; \omega) = \sum_{m=0}^{p-1} a_m \omega^m, \quad (56)$$

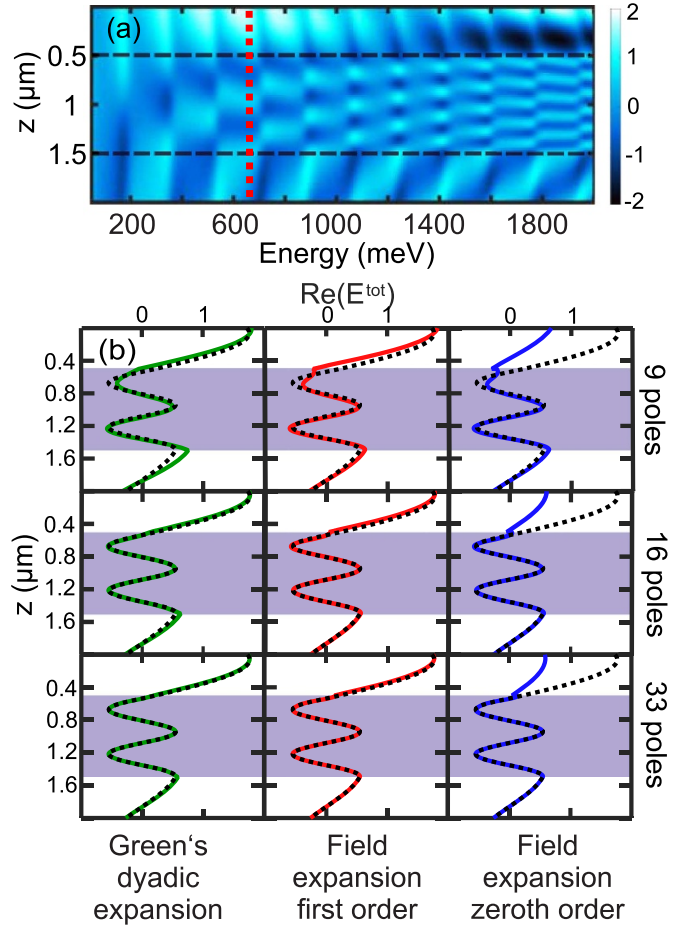


Figure 4. Near field in a dielectric slab with refractive index $n = 3.5$ and thickness $1 \mu\text{m}$ in air. Panel (a) displays the analytic near field as a function of photon energy. In panel (b), the comparison of different formulations for the pole expansion of the near field is shown at a photon energy of 650 meV (red dashed line in (a)): the results on the left have been calculated via equation (53). The other results have been obtained using equation (55) in its first- (middle) and zeroth-order (right) formulation. From top to bottom, the number of poles is increased from 9 over 17 to 33. The dotted lines denote the analytic result. All approaches converge to the analytic result, except for the zeroth-order formulation, which cannot be applied at the top interface. Reprinted with permission from [106] © The Optical Society.

$$a_m = \frac{\mathbb{F}_{\text{tot}}^{(m)}(\mathbf{r}; 0)}{m!} - \sum_n \frac{I_n(\omega_n)}{\omega_n^{m+1}} \mathbb{F}_n(\mathbf{r}). \quad (57)$$

Here, $\mathbb{F}_{\text{tot}}^{(m)}$ denotes the m th derivative of \mathbb{F} with respect to ω . Evidently, the pole contribution in equation (55) is much simpler than that in equation (53), since it requires calculating the overlap integral in equation (54) only once at the complex frequencies ω_n of the poles. The drawback is that we need to account for a more complex background. A comparison of equation (53) with the zeroth- and first-order version of equation (55) is displayed in figure 4 for the example of a planar dielectric slab. It can be seen that the zeroth-order version fails at the top interface, because the asymptotic behavior of the total field at the top interface

prevents the application of the zeroth-order Mittag-Leffler expansion [106].

At the end of this subsection, we would like to sketch an alternative derivation for the pole contribution in equation (55) from equation (52) that does not require the pole expansion of the Green's dyadic and yields directly the correct normalization. First, we multiply equation (52) from the left with \mathbb{F}_n^\dagger . Then, we subtract a zero in the form $\mathbb{F}_{\text{scat}} \cdot \hat{\mathbb{M}}^\dagger(\omega_n) \mathbb{F}_n^\dagger$, which yields:

$$\mathbb{F}_n^\dagger \cdot \left[\frac{\omega}{c} \hat{\mathbb{P}}(\omega) - \frac{\omega_n}{c} \hat{\mathbb{P}}(\omega_n) \right] \mathbb{F}_{\text{scat}} - \mathbb{F}_n^\dagger \cdot \hat{\mathbb{D}} \mathbb{F}_{\text{scat}} + \mathbb{F}_{\text{scat}} \cdot \hat{\mathbb{D}} \mathbb{F}_n^\dagger = -\frac{\omega}{c} \mathbb{F}_n^\dagger \cdot \hat{\Delta} \hat{\mathbb{P}}(\omega) \mathbb{F}_{\text{BG}}. \quad (58)$$

The expression in the first line vanishes at ω_n . In order to obtain finite results for the scattered field, we therefore assume that the scattered field can be expanded as:

$$\mathbb{F}_{\text{scat}} = -c \sum_n \frac{b_n(\omega)}{\omega - \omega_n} \mathbb{F}_n. \quad (59)$$

The factor $-c$ has been introduced for the sake of consistency with the next section. By integrating over equation (58) and using the orthogonality relation in equation (48), we then obtain in the limit $\omega \rightarrow \omega_n$:

$$b_n(\omega_n) = \frac{1}{c} \frac{I_n(\omega_n)}{V_n + S_n}. \quad (60)$$

The expressions V_n and S_n in the denominator are defined in equations (37) and (38). In the case that the resonant field distributions are normalized, their sum equals unity, see equation (36).

This derivation resembles that of the so-called orthogonality decomposition [94]. The orthogonality decomposition is based on the assumption that the scattered field can be decomposed everywhere in terms of the RS \mathbb{F}_n when using perfectly-matched layers. Then, the modal expansion is introduced as $\mathbb{F}_{\text{scat}} = \sum_n a_n(\omega) \mathbb{F}_n$, and an integral over equation (58) is carried out that spans over the entire space \tilde{V} with perfectly-matched layers, so that any occurring surface integrals vanish in that limit. Then, one obtains a matrix operator that needs to be regularized for dispersive media and inverted in order to calculate the coefficients a_n [3]. However, it turns out that such an expansion is only appropriate if we add numerical solutions to the set of RS that are predominantly localized in the region of perfectly-matched layer and do not have any physical counterpart in a system without perfectly-matched layers [10].

2.6. Completeness

The question arises if any of the aforementioned modal expansions converges properly and what are the limitations. Most importantly, is the basis of RS actually complete? Regarding the spatial domain of completeness, it is obvious that equation (50) cannot be correct over the entire space. The reason is that fields generated by a local source at a real-valued frequency remain in general finite—particularly far away from the source. However, the resonant field distributions grow

with distance to the resonator. The attempt of expressing a finite field by using only exponentially growing functions is condemned to fail. Kristensen and coworkers identify a so-called region of consistency in the vicinity of the resonator, in which the expansion in terms of RS gives reasonably accurate results [95], but strictly speaking, the pole expansion of the Green's dyadic in equation (29) is only valid inside the resonator and at its outermost interfaces. When using perfectly-matched layers, the non-physical modes that are localized in the regions of perfectly-matched layers have to be included to ensure completeness [10].

Another question is that of the completeness in the interior. While the closure relation given by equation (30) yields the necessary condition for a complete basis, the sum rules in equation (32) indicate that the basis of RS can be overcomplete. This fact was already noted in the context of RS in quantum mechanics [96, 132]. An open question in this context is the completeness in the presence of exceptional points, where we find fewer linear independent resonant field distributions than eigenfrequencies.

It should be also mentioned that there is often another contribution to the pole expansion of the Green's dyadic. More specifically, the analytic continuation of the Green's dyadic to the complex frequency plane may contain cuts that arise, e.g. due to selecting appropriate Riemann sheets in the case of complex square roots [83, 105]. In this general case, the Green's dyadic can be expanded as [12, 83, 87]:

$$\hat{\mathbb{G}}(\mathbf{r}, \mathbf{r}'; \omega) = c \sum_n \frac{\mathbb{F}_n(\mathbf{r}) \otimes \mathbb{F}_n^\dagger(\mathbf{r}')}{\omega - \omega_n} + \sum_m \hat{\mathbb{G}}_m(\mathbf{r}, \mathbf{r}'; \omega), \quad (61)$$

where m labels the individual cut contributions with:

$$\hat{\mathbb{G}}_m(\mathbf{r}, \mathbf{r}'; \omega) = \frac{1}{2\pi i} \int_{C_m} d\omega' \frac{\Delta \hat{\mathbb{G}}(\mathbf{r}, \mathbf{r}'; \omega')}{\omega - \omega'}, \quad (62)$$

with C_m denoting a path along the m th cut and $\Delta \hat{\mathbb{G}}$ being the difference between the Green's dyadic on the different Riemann sheets. In numerical calculations, these cut contributions can be discretized [87], and single cuts can be circumvented by using analytic continuations over other parameters than complex frequency [17, 105]. Furthermore, in systems surrounded by perfectly-matched layers, these cut contributions disappear and are replaced by a bunch of numerical modes [10, 94]. However, a general analytical treatment of arbitrary cut contributions is still to be developed.

Finally, there is another issue arising due to the discontinuities of the electric and magnetic fields. Whenever it is required to expand quantities with discontinuities by basis functions that exhibit no appropriate discontinuities, the convergence of this expansion will suffer from the Gibbs phenomenon, which is well-understood in the framework of numerical calculations via the Fourier-modal method [133–136]. When using RS as basis, a possible solution is to include so-called static modes [98], which are not solutions of Maxwell's equations in a physical sense. This aspect will be discussed later in section 3.1.

2.7. Far-field expansion

In the following, we show how the optical far-field response of a resonator can be calculated from its RS. Owing to its high practical relevance, we focus on the calculation of the optical scattering matrix [9, 13, 21–23]; however, the presented approach can also be extended to other quantities, such as the radiation diagram of emitters located inside the resonator [137].

Let us choose a surface ∂V that surrounds the resonator. On this surface, one can construct complete and orthogonal sets of incoming $\{\mathbb{I}_N\}$ and outgoing $\{\mathbb{O}_N\}$ basis functions [8, 13]. The vector \mathbf{N} is the same as introduced in section 2.3 and summarizes all labels needed to specify the basis functions (e.g. their polarization and propagation direction). Every incoming basis function \mathbb{I}_N has an outgoing counterpart \mathbb{O}_N . With the help of the basis functions, an arbitrary field \mathbb{F} can be decomposed as:

$$\mathbb{F}(\mathbf{r}; \omega) = \sum_{\mathbf{N}} \alpha_{\mathbf{N}}^{\text{in}}(\omega) \mathbb{I}_{\mathbf{N}}(\mathbf{r}; \omega) + \alpha_{\mathbf{N}}^{\text{out}}(\omega) \mathbb{O}_{\mathbf{N}}(\mathbf{r}; \omega), \quad (63)$$

where $\alpha_{\mathbf{N}}^{\text{in}}$ and $\alpha_{\mathbf{N}}^{\text{out}}$ denote expansion coefficients on the surface ∂V .

The basis functions $\mathbb{I}_N = (\mathbf{E}_{\text{in},N}; i\mathbf{H}_{\text{in},N})^T$ and $\mathbb{O}_N = (\mathbf{E}_{\text{out},N}; i\mathbf{H}_{\text{out},N})^T$ can be chosen such that they fulfill the following orthogonality relations [13]:

$$i \oint_{\partial V} d\mathbf{S} \cdot (\mathbf{E}_{\text{in},N}^{\dagger} \times \mathbf{H}_{\text{out},M} - \mathbf{E}_{\text{out},M} \times \mathbf{H}_{\text{in},N}^{\dagger}) = \delta_{NM}, \quad (64)$$

$$i \oint_{\partial V} d\mathbf{S} \cdot (\mathbf{E}_{\text{in},N} \times \mathbf{H}_{\text{out},M}^{\dagger} - \mathbf{E}_{\text{out},M}^{\dagger} \times \mathbf{H}_{\text{in},N}) = \delta_{NM}, \quad (65)$$

$$i \oint_{\partial V} d\mathbf{S} \cdot (\mathbf{E}_{\text{in},N}^{\dagger} \times \mathbf{H}_{\text{in},M} - \mathbf{E}_{\text{in},M} \times \mathbf{H}_{\text{in},N}^{\dagger}) = 0, \quad (66)$$

$$i \oint_{\partial V} d\mathbf{S} \cdot (\mathbf{E}_{\text{out},N}^{\dagger} \times \mathbf{H}_{\text{out},M} - \mathbf{E}_{\text{out},M} \times \mathbf{H}_{\text{out},N}^{\dagger}) = 0. \quad (67)$$

Consequently, the expansion coefficients in equation (63) become:

$$\alpha_{\mathbf{N}}^{\text{in}} = -i \oint_{\partial V} d\mathbf{S} \cdot (\mathbf{E}_{\text{out},N}^{\dagger} \times \mathbf{H} - \mathbf{E} \times \mathbf{H}_{\text{out},N}^{\dagger}), \quad (68)$$

$$\alpha_{\mathbf{N}}^{\text{out}} = i \oint_{\partial V} d\mathbf{S} \cdot (\mathbf{E}_{\text{in},N}^{\dagger} \times \mathbf{H} - \mathbf{E} \times \mathbf{H}_{\text{in},N}^{\dagger}). \quad (69)$$

Note that a missing minus sign from [13] is corrected for in equation (68). Also, we would like to mention that the normalized resonant field distributions \mathbb{F}_n have units $\text{m}^{-3/2}$, while equations (64) and (65) imply that \mathbb{I}_N and \mathbb{O}_M have units m^{-1} . For the sake of consistency, we assume now that all fields except \mathbb{F}_n are given in units m^{-1} . The results can be translated to any other units by multiplying the fields with an appropriate factor.

The interaction of a resonator with incoming and outgoing basis functions can be summarized in its scattering matrix S . For an arbitrary incident field, written as $\mathbb{F}^{(\text{in})} = \sum_{\mathbf{N}} \alpha_{\mathbf{N}}^{\text{in}} \mathbb{I}_{\mathbf{N}}$, the response of the resonator, written as $\mathbb{F}^{(\text{out})} = \sum_{\mathbf{N}} \alpha_{\mathbf{N}}^{\text{out}} \mathbb{O}_{\mathbf{N}}$, is given by:

$$\alpha_{\mathbf{M}}^{\text{out}} = \sum_{\mathbf{N}} S_{\mathbf{MN}} \alpha_{\mathbf{N}}^{\text{in}}, \quad (70)$$

where $S_{\mathbf{MN}}$ denote the corresponding elements of the scattering matrix. It should be mentioned that in the context of the scattering matrix, the indices \mathbf{M} and \mathbf{N} are often referred to as channels.

Let us now calculate the elements $S_{\mathbf{MN}}$. We assume that the resonator is excited via a basis function $\mathbb{I}_N(\omega)$. This generates the following fields:

$$\mathbb{F}_{\text{tot},N}(\omega) = \mathbb{F}_{\text{BG},N}(\omega) + \mathbb{F}_{\text{scat},N}(\omega). \quad (71)$$

The elements $S_{\mathbf{MN}}$ are then obtained by applying equation (69) for the channel \mathbf{M} to equation (71). This yields:

$$S_{\mathbf{MN}}(\omega) = S_{\mathbf{MN}}^{\text{BG}}(\omega) + S_{\mathbf{MN}}^{\text{scat}}(\omega), \quad (72)$$

with the scattering matrix of the background system:

$$S_{\mathbf{MN}}^{\text{BG}}(\omega) = i \oint_{\partial V} d\mathbf{S} \cdot \left[\mathbf{E}_{\text{in},M}^{\dagger}(\omega) \times \mathbf{H}_{\text{BG},N}(\omega) - \mathbf{E}_{\text{BG},N}(\omega) \times \mathbf{H}_{\text{in},M}^{\dagger}(\omega) \right], \quad (73)$$

which only contains fields that are assumed to be known and can directly be calculated, and a contribution:

$$S_{\mathbf{MN}}^{\text{scat}}(\omega) = i \oint_{\partial V} d\mathbf{S} \cdot \left[\mathbf{E}_{\text{in},M}^{\dagger}(\omega) \times \mathbf{H}_{\text{scat},N}(\omega) - \mathbf{E}_{\text{scat},N}(\omega) \times \mathbf{H}_{\text{in},M}^{\dagger}(\omega) \right], \quad (74)$$

which contains the yet unknown scattered field and will be evaluated in the following. We will present two alternative approaches for this evaluation, resulting in two alternative representations of the scattering matrix.

2.7.1. Asymmetric representation. We start with equation (74), use the expansion of the scattered field given by equation (59), and insert the result back into equation (72). This yields the following expansion of the scattering matrix [13]:

$$S_{\mathbf{MN}}(\omega) = S_{\mathbf{MN}}^{\text{BG}}(\omega) - c \sum_n \frac{\alpha_{\mathbf{M}}^{(n)}(\omega) b_{\mathbf{N}}^{(n)}(\omega)}{\omega - \omega_n}. \quad (75)$$

In this case, the weight function of each pole contribution is frequency-dependent, with:

$$\alpha_{\mathbf{M}}^{(n)}(\omega) = i \oint_{\partial V} d\mathbf{S} \cdot \left[\mathbf{E}_{\text{in},M}^{\dagger}(\omega) \times \mathbf{H}_n - \mathbf{E}_n \times \mathbf{H}_{\text{in},M}^{\dagger}(\omega) \right], \quad (76)$$

and

$$b_{\mathbf{N}}^{(n)}(\omega) = \frac{\omega}{c} \int_V dV \mathbb{F}_n^\dagger \cdot \Delta \hat{\mathbb{P}}(\omega) \mathbb{F}_{\text{BG},\mathbf{N}}(\omega). \quad (77)$$

Here, $\alpha_{\mathbf{M}}^{(n)}$ and $b_{\mathbf{N}}^{(n)}$ can be interpreted as the emission and excitation coefficients of resonant state \mathbb{F}_n , respectively. The Greek letter $\alpha_{\mathbf{M}}^{(n)}$ is used in contrast to the Latin letter $b_{\mathbf{N}}^{(n)}(\omega)$, to emphasize that the former contains a surface integral, while the latter contains a volume integral. Owing to this asymmetry, we refer to equation (75) as the asymmetric representation.

2.72. Symmetric representation. We take equation (74) and replace $\mathbb{I}_{\mathbf{M}}^\dagger$ with the background field $\mathbb{F}_{\text{BG},\mathbf{M}}^\dagger$ that it would generate when being launched into the resonator. One can easily verify that this replacement is possible by noting that on the surface ∂V , $\mathbb{F}_{\text{scat},\mathbf{N}}$ is a superposition of outgoing basis functions, while $\mathbb{F}_{\text{BG},\mathbf{M}}^\dagger$ is a superposition of $\mathbb{I}_{\mathbf{M}}^\dagger$ with some outgoing basis functions, and further using the orthogonality relations from equations (65) and (67). Then, we apply equation (22) to convert the surface integral into a volume integral. After some algebra [138], this gives:

$$S_{\text{MN}}^{\text{scat}}(\omega) = -\frac{\omega}{c} \int_V dV \left[\mathbb{F}_{\text{BG},\mathbf{M}}^\dagger(\omega) \cdot \Delta \hat{\mathbb{P}}(\omega) \mathbb{F}_{\text{tot},\mathbf{N}}(\omega) \right]. \quad (78)$$

Here, $\mathbb{F}_{\text{tot},\mathbf{N}}$ is the sum of background and scattered field of channel \mathbf{N} , see equation (71). Applying the expansion of the scattered field as formulated in equation (59) into equation (78), and inserting the result back into equation (72) yields the following alternative formulation of the scattering matrix [22, 138]:

$$S_{\text{MN}}(\omega) = S_{\text{MN}}^{\text{BG}}(\omega) + S_{\text{MN}}^{\text{Born}}(\omega) + c \sum_n \frac{\alpha_{\mathbf{M}}^{(n)}(\omega) b_{\mathbf{N}}^{(n)}(\omega)}{\omega - \omega_n}. \quad (79)$$

Comparing this result with equation (75), we note the additional background term:

$$S_{\text{MN}}^{\text{Born}}(\omega) = -\frac{\omega}{c} \int_V dV \mathbb{F}_{\text{BG},\mathbf{M}}^\dagger(\omega) \cdot \Delta \hat{\mathbb{P}}(\omega) \mathbb{F}_{\text{BG},\mathbf{N}}(\omega), \quad (80)$$

and the modified numerator with $b_{\mathbf{M}}^{(n)}(\omega)$ known from equation (77) and,

$$a_{\mathbf{M}}^{(n)}(\omega) = \frac{\omega}{c} \int_V dV \mathbb{F}_{\text{BG},\mathbf{M}}^\dagger(\omega) \cdot \Delta \hat{\mathbb{P}}(\omega) \mathbb{F}_n. \quad (81)$$

Since equation (79) contains emission and excitation coefficients $a_{\mathbf{M}}^{(n)}$ and $b_{\mathbf{N}}^{(n)}$, respectively, that are both defined via volume integrals, we refer to it as the symmetric representation. In contrast to the asymmetric representation, it contains the additional term $S_{\text{MN}}^{\text{Born}}$, which comprises an overlap integral between the two background fields and can be interpreted as a Born-like scattering interaction [22]. In [22], an alternative derivation of the symmetric representation is provided, which

is based on the orthogonality-decomposition approach [94]. In this work, it is claimed that the asymmetric representation derived in [13] is incomplete. This appears, however, to be a misinterpretation, since, as shown above, both representations are equally valid and can be converted from one to the other. Furthermore, it should be mentioned that, instead of expanding only \mathbb{F}_{scat} inside the resonator in terms of the RS while keeping \mathbb{F}_{BG} as it is, one can also expand the total field \mathbb{F}_{tot} , leading to a third and equally valid scattering-matrix representation [9].

2.73. Simplified ω dependence. All scattering-matrix expansions discussed so far have the drawback that they contain ω -dependent overlap integrals. This may slow down practical computations, since the integrals have to be evaluated repeatedly. In analogy to the near-field case, the ω dependence can be removed by considering $S_{\text{MN}}(\omega)$ as a function that is analytic in ω , except for a countable number of poles, and applying the Mittag-Leffler theorem once more. Note that, as in the near-field case, the prerequisites have to be checked, especially regarding the asymptotic behavior of $S_{\text{MN}}(\omega)$ for $\omega \rightarrow \infty$. In some situations, such as that of the analytic Mie theory [139], the requirement on this asymptotic behavior is not fulfilled in the conventional definition of the scattering matrix. However, it is possible to apply the Mittag-Leffler theorem, if one performs a regularization for the scattering matrix beforehand [140].

We will now show the application of the Mittag-Leffler theorem for the example of the asymmetric representation from equation (75). An analogous procedure can be applied to the other formulations (a detailed discussion for the case of the symmetric formulation, e.g. can be found in [22]). We start with equation (75) and apply the Mittag-Leffler theorem. Then, we replace the volume integral in equation (77) via simple algebra by a surface integral using [13]:

$$b_{\mathbf{N}}^{(n)}(\omega_n) = \beta_{\mathbf{N}}^{(n)}(\omega_n), \quad (82)$$

with

$$\beta_{\mathbf{N}}^{(n)}(\omega) = i \oint_{\partial V} d\mathbf{S} \cdot \left[\mathbf{E}_n^\dagger(\omega) \times \mathbf{H}_{\text{in},\mathbf{N}} - \mathbf{E}_{\text{in},\mathbf{N}} \times \mathbf{H}_n^\dagger(\omega) \right]. \quad (83)$$

Assuming a resonance-free background system, this gives (compare equations (55)–(57) for the near-field case) [13]:

$$S_{\text{MN}}(\omega) = S_{\text{MN}}^p(\omega) - c \sum_n \frac{\alpha_{\mathbf{M}}^{(n)}(\omega_n) \beta_{\mathbf{N}}^{(n)}(\omega_n)}{\omega - \omega_n}, \quad (84)$$

where $S_{\text{MN}}^0 = 0$, while S_{MN}^p is a polynomial of order $p - 1$:

$$S_{\text{MN}}^p(\omega) = \sum_{m=0}^{p-1} A_{\text{MN}}^{(m)} \omega^m, \quad (85)$$

with matrix coefficients:

$$A_{\text{MN}}^{(m)} = \frac{S_{\text{MN}}^p(0)}{m!} - c \sum_n \frac{\alpha_{\mathbf{M}}^{(n)}(\omega_n) \beta_{\mathbf{N}}^{(n)}(\omega_n)}{\omega_n^{m+1}}. \quad (86)$$

Here, $S_{MN}^{(m)}$ denotes the m th derivative of S_{MN} with respect to ω . The advantage of equation (84) is a highly simplified ω dependence, where the excitation and emission coefficients have to be evaluated only once at the complex frequencies ω_n . The price to pay is, however, that one needs to deal with a more sophisticated background term S_{MN}^p .

In analytically solvable systems (e.g. those in [13, 22]), the background term can be determined via its defining equation. In numerical calculations, however, this can be difficult, especially due to the occurrence of the ω derivatives. A highly practical approach consists in including only a small number of poles in the expansion (enough to accurately resolve all relevant features in some spectral region of interest) and accounting for S_{MN}^p , as well as for the influence of other poles by some simple background polynomial, which can be fitted, e.g. from numerically exact calculations [13]. As an alternative to the fit, one can also establish symmetry constraints for the scattering matrix, and introduce a weighting of the coefficients that minimizes the error in the expansion [21]. This latter approach was recently refined by also taking energy conservation into account [23]. For single RS, this regularization can be achieved even analytically, as shown already in 2005 by Gippius *et al* [141]. Another alternative in order to account for the influence of such a background as well as for that of remaining poles consists in the use of a Riesz-projection method [137, 142]. An important benefit of all of the above approaches is that they allow to accurately resolve resonant spectral features, while at the same time keeping the computational efforts very low compared to, e.g. full numerical calculations. An interesting open question to be answered is which method does provide the best convergence performance for which kind of application.

Figure 5 displays the comparison of full-wave calculations by the Fourier-modal method [127, 128] with the pole expansion of the scattering matrix obtained by equation (84) for the case of a one-dimensional photonic crystal slab. The example is taken from [13], where four RS located at 2676.2–0.2i meV, 3180.0–92.7i meV, 3719.3–9.7i meV, and 3854.7–0.7i meV have been considered together with a cubic fit for the background. While it can be cumbersome to resolve the sharp resonant features in the spectra with conventional numerical calculations, the pole expansion yields the correct spectral behavior at low computational cost.

When looking at the spectral lineshapes in figure 5, we can see that the resonant features not only differ in the resonant linewidth, but also the shape changes between the four resonances. Taking only a single pole contribution from equation (84), one would expect that each resonant state is manifested as a Lorentzian in the spectra. However, the interplay between the various RS and the background results in the rich diversity of spectral lineshapes. A good overview of the classification of resonant lineshapes and their physical origin can be found in [143]. One prominent example is that of a Fano resonance [27, 144–147], which can be also observed in figure 5 with the typical asymmetry due to the interplay between the background and the resonant contribution. Fano lineshapes arise due to the coupling of a continuum with a

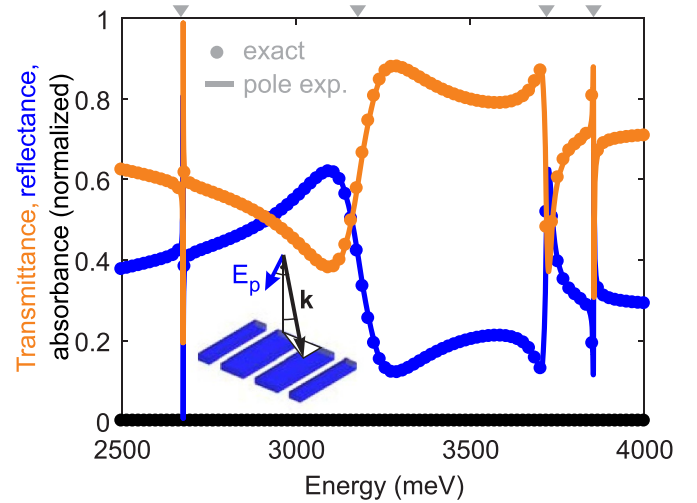


Figure 5. Pole expansion of the transmittance (orange), reflectance (blue), and absorbance (black) for p-polarized incidence at $k_x = k_y = 0.2 \mu\text{m}^{-1}$ in the case of a one-dimensional photonic crystal slab. Numerically exact results are shown by dots, while the pole expansion with four RS and a cubic background fit is given by solid lines. The real part of the complex eigenfrequencies is indicated by the gray triangles at the top. Reprinted figure with permission from [13], Copyright (2018) by the American Physical Society.

single resonant state or the coupling of a broad optically active resonant state and a resonant state that is optically inactive [143]. A special case for Fano resonances is that of electromagnetically induced transparency, which occurs in the weak coupling regime between two RS with identical real parts of the eigenfrequencies [143, 148–150].

3. Applications

3.1. Resonant-state expansion

One of the first applications of the analytic mode normalization of RS was the resonant-state expansion as a perturbative method up to any orders of perturbation [1]. The starting point is a system with material distribution $\hat{\mathbb{P}}_0$ that exhibits a known set of RS with eigenfrequencies ω_n and field distributions \mathbb{F}_n , which will be used as basis functions. Then, we consider a perturbed system with material distribution $\hat{\mathbb{P}}_0 + \delta\hat{\mathbb{P}}$, where $\delta\hat{\mathbb{P}}$ denotes the perturbation. Substituting this material distribution into equation (11), we obtain for the new RS \mathbb{F}_ν of the perturbed system with eigenfrequencies ω_ν :

$$\hat{\mathbb{M}}_0(\mathbf{r}; \omega_\nu) \mathbb{F}_\nu(\mathbf{r}) = -\frac{\omega_\nu}{c} \delta\hat{\mathbb{P}}(\mathbf{r}; \omega_\nu) \mathbb{F}_\nu(\mathbf{r}). \quad (87)$$

Here, $\hat{\mathbb{M}}_0 = k\hat{\mathbb{P}}_0 - \hat{\mathbb{D}}$ is the Maxwell operator of the unperturbed system. Knowing the pole expansion of its Green's dyadic according to equation (29) and assuming that $\delta\hat{\mathbb{P}}$ is sufficiently localized to warrant the validity of this pole expansion, we can thus formally invert equation (87) and write [1, 91]:

$$\mathbb{F}_\nu(\mathbf{r}) = \sum_n \frac{-\omega_\nu \mathbb{F}_n(\mathbf{r})}{\omega_\nu - \omega_n} \int_V dV' \mathbb{F}_n^\dagger(\mathbf{r}') \cdot \delta \hat{\mathbb{P}}(\mathbf{r}'; \omega_\nu) \mathbb{F}_\nu(\mathbf{r}'). \quad (88)$$

Finally, we express \mathbb{F}_ν as $\mathbb{F}_\nu = \sum_n b_n \mathbb{F}_n$ and insert this on both sides of equation (88). Since the result must be valid at any position \mathbf{r} and independently of $\delta \hat{\mathbb{P}}$, this yields:

$$(\omega_\nu - \omega_n) b_n = -\omega_\nu \sum_m V_{nm}(\omega_\nu) b_m, \quad (89)$$

where

$$V_{nm}(\omega_\nu) = \int_V dV' \mathbb{F}_n^\dagger(\mathbf{r}') \cdot \delta \hat{\mathbb{P}}(\mathbf{r}'; \omega_\nu) \mathbb{F}_m(\mathbf{r}'). \quad (90)$$

If $\delta \hat{\mathbb{P}}$ is non-dispersive, i.e. it does not depend on ω , we thus obtain a general linear eigenvalue problem in the form of equation (89), which is the resonant-state expansion in its simplest form.

Assuming instead a perturbation of a general Drude–Lorentz from as in equation (31), with:

$$\delta \hat{\mathbb{P}}(\mathbf{r}; \omega) = \delta \hat{\mathbb{P}}_\infty(\mathbf{r}) + \sum_j \frac{\delta \hat{\mathbb{Q}}_j(\mathbf{r})}{\omega - \Omega_j}, \quad (91)$$

we can obtain after some algebra the dispersive formulation of the resonant-state expansion [91]:

$$\begin{aligned} (\omega_\nu - \omega_n) b_n &= -\omega_\nu \sum_m V_{nm}(\infty) b_m \\ &+ \omega_n \sum_m [V_{nm}(\infty) - V_{nm}(\omega_n)] b_m. \end{aligned} \quad (92)$$

It should be noted that both the dispersive and the non-dispersive resonant-state expansion have been initially derived for non-magnetic systems [1, 6]. In that case, the perturbation is solely given by a change $\delta \varepsilon$ in the permittivity. It has been first demonstrated for perturbations of a dielectric slab and a microsphere [1, 5, 16]. Later, it has been extended to dielectric cylinders [87] and microcavities [20] as well as one- and two-dimensional periodic arrays [12]. The first dispersive formulation is given in [6], where the RS of a dielectric sphere have been used to calculate the RS of a gold sphere. This is highly beneficial, because calculating the RS of a dielectric sphere turns out to be much simpler than finding all relevant RS of a metallic sphere.

As discussed above in section 2.6, there is another possible contribution to the Green's dyadic, which is cuts in the complex frequency plane. In [17], these cut contributions are circumvented in a dielectric slab by considering the wavevector component k_z perpendicular to the slab as new variable for an analytic continuation to the complex plane instead of the frequency. In that case, the exact coefficients of transmission and reflection contain the frequency under a square root, see equation (15), which leads to the cut contributions, while the dependence on k_z is unambiguous and free of cuts. In other publications, the continuous frequency dependence of the cuts

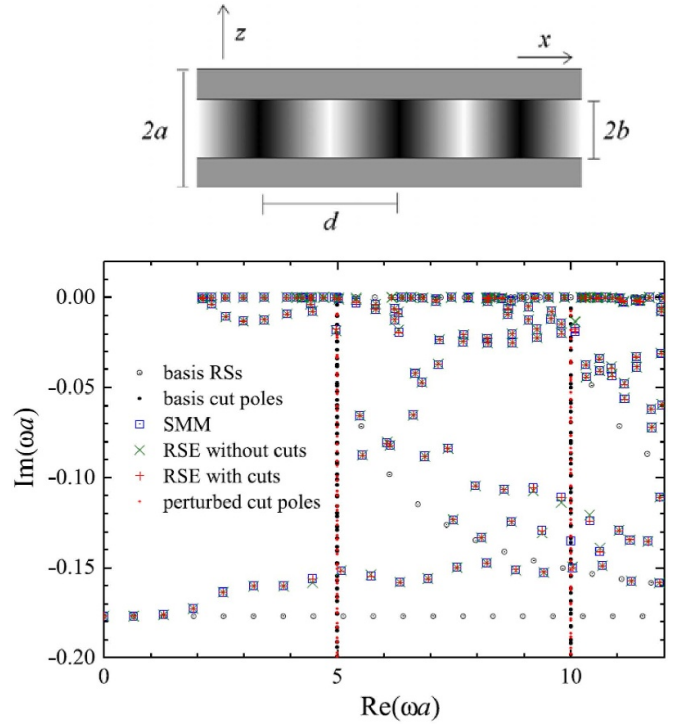


Figure 6. Resonant-state expansion for constructing the RS of a one-dimensional periodic modulated slab of thickness $2b = a$ and period $d = 2\pi a/5$ from those of a homogeneous and isotropic slab of thickness $2a$ in air. The permittivity modulation of the periodic system is sinusoidal with an amplitude of ± 1 ; the background permittivity is $\varepsilon = 6$. The top panel depicts a schematic of the system, while the bottom panel displays the complex eigenfrequencies of the perturbed and unperturbed system. Large and small black dots are the basis resonant states (RSs) and cut poles, respectively, while the blue squares denote the RS of the perturbed system. The results of resonant-state expansion with basis cut poles (red pluses) agrees better with the exact results of the perturbed system than those without cuts (green crosses) for the same number of Bragg harmonics ($M = 5$) and yields perturbed cut poles (red dots). Reprinted figure with permission from [66], Copyright (2018) by the American Physical Society.

given in equation (62) is discretized in the form of a finite set of equivalent cut poles [65, 66, 83, 87]. For instance, the Muljarov group has shown recently that it is even possible to construct the RS of one-dimensional periodic arrays from the RS of a dielectric slab [65, 66], see figure 6. The discretized cuts are denoted by small dots. In the case that the cuts are far enough away from the spectral region of interest, they can be often ignored completely. Using this formalism, Neale and Muljarov investigated the occurrence of symmetry-protected and accidental bound states in the continuum and developed a criterion for distinguishing them: Symmetry-protected bound states in the continuum can be understood as a superposition of slab modes that do not radiate to the far field, while accidental bound states in the continuum arise as a superposition of several radiative slab modes such that the radiation to the far field is canceled out.

Another issue that has been mentioned in section 3.1 is that there exists a set of solutions of equation (11) at $\omega_n = 0$, which

are not physical solutions of Maxwell's equations. Instead, these solutions obey [98, 151]:

$$\nabla \times \mathbf{E}_\lambda = 0, \quad (93)$$

$$\nabla \times \mathbf{H}_\lambda = 0. \quad (94)$$

These equations are completely independent, so that we can derive two subclasses of static modes [151]:

$$\mathbf{E}_\lambda^{\text{LE}} = -\nabla\psi_\lambda^{\text{LE}}, \quad \mathbf{H}_\lambda^{\text{LE}} = 0, \quad (95)$$

$$\mathbf{H}_\lambda^{\text{LM}} = -\nabla\psi_\lambda^{\text{LM}}, \quad \mathbf{E}_\lambda^{\text{LM}} = 0. \quad (96)$$

Here, ψ_λ^{LE} and ψ_λ^{LM} are the potentials of longitudinal electric (LE) and longitudinal magnetic (LM) static modes. Since these modes are no solutions of the divergence equations:

$$\nabla \cdot (\varepsilon \mathbf{E} + \xi \mathbf{H}) = 0, \quad (97)$$

$$\nabla \cdot (\zeta \mathbf{E} + \mu \mathbf{H}) = 0, \quad (98)$$

they do not necessarily obey Maxwell's boundary conditions for fields at interfaces between two materials. Therefore, adding the static modes as poles at $\omega = 0$ to the expansion of the Green's dyadic in equations (29) or (61) can result in a much better convergence of the resonant-state expansion in the case that the boundary conditions change between the initial and the perturbed system [98, 151]. For instance, it is shown in [98] how to derive the RS of a cylindrical disk from those of a spherical resonator. The static modes are normalized by the condition $V_n = 1$, where V_n is defined in equation (37) and the integration is taken over the entire space. Furthermore, it is shown in [151] how to eliminate static modes in the expansion of the Green's dyadic at the cost of an additional δ function. However, it should be noted that static modes have been considered so far only for dielectric systems.

3.2. First-order perturbation theory and sensing

In recent times, sensing has become one of the key applications of nanophotonics [24, 32–34, 152–155]. Here, one is typically interested in detecting tiny changes in some nanophotonic system that are induced by the presence of an analyte medium. For the theoretical description of such interactions, it is highly useful to treat these changes via a first-order perturbation theory [5, 11, 12, 14, 26, 27, 138]. First, this approach is very efficient from a computational point of view. Second, it can provide deep intuitive insights into the heart of the interaction, which are, e.g. useful for sensor design and optimization.

In the first part of this subsection, we focus on perturbation-induced frequency shifts, which denote the basis for a large number of sensing schemes. In the second part, we go one step further, and consider the impact of perturbations onto optical far-field properties, represented by the optical

scattering matrix. Note that we consider here only material changes, as they are relevant in sensing, but do not discuss shape deformations of the resonator, which may require another type of perturbation theory to be treated in a similar manner [151, 156, 157]

Let us now develop an expression for the change in the eigenfrequencies ω_n of a resonator under weak changes of its material distribution. In principle, the result is already contained in the resonant-state expansion from the previous subsection. One can simply take the eigenvalue equations of the resonant-state expansion and apply a first-order approximation in the perturbation $\delta\hat{\mathbb{P}}$, resulting in a simple closed-form expression for the change of ω_n [5, 11, 12, 20, 26]. However, this approach is restricted to perturbations inside or in the vicinity of the resonator. In order to be more general, we show here the derivations from [14], which additionally allow to account for the case that the perturbation $\delta\hat{\mathbb{P}}$ includes homogeneous and isotropic perturbations in the resonator's surrounding.

First, the RS of the perturbed system obey the following equation:

$$\left[\hat{\mathbb{M}}_0(\mathbf{r}; \omega_\nu) + \Lambda \frac{\omega_\nu}{c} \delta\hat{\mathbb{P}}(\mathbf{r}; \omega_\nu) \right] \mathbb{F}_\nu = 0. \quad (99)$$

Here, $\hat{\mathbb{M}}_0$ is the Maxwell operator of the unperturbed system, ω_ν is the perturbed resonance frequency, and \mathbb{F}_ν the corresponding field distribution. In analogy to conventional perturbation theories (e.g. known from quantum mechanics [158]), we introduce the perturbation parameter Λ , which is assumed to be small. From a conceptual standpoint, however, we can turn the perturbation on ($\Lambda = 1$) or off ($\Lambda = 0$).

Multiplying equation (99) with \mathbb{F}_n^\dagger and subtracting \mathbb{F}_ν times equation (28) of the unperturbed system, we obtain via equation (22):

$$\begin{aligned} & \int_V dV \mathbb{F}_n^\dagger \cdot \left[\omega_\nu \hat{\mathbb{P}}(\omega_\nu) - \omega_n \hat{\mathbb{P}}(\omega_n) \right] \mathbb{F}_\nu \\ & + \Lambda \omega_\nu \int_V dV \mathbb{F}_n^\dagger \cdot \delta\hat{\mathbb{P}}(\omega_\nu) \mathbb{F}_\nu \\ & + ic \oint_{\partial V} d\mathbf{S} \cdot (\mathbf{E}_n^\dagger \times \mathbf{H}_\nu - \mathbf{E}_\nu \times \mathbf{H}_n^\dagger) = 0. \end{aligned} \quad (100)$$

Then, we assume that the perturbation is small and expand all quantities as perturbation series in powers of Λ :

$$\mathbb{F}_\nu = \mathbb{F}_n + \Lambda \mathbb{F}_n^{(1)} + \mathcal{O}(\Lambda^2), \quad (101)$$

$$\omega_\nu = \omega_n + \Lambda \omega_n^{(1)} + \mathcal{O}(\Lambda^2). \quad (102)$$

When inserting these relations into equation (100) and sorting the result by powers of Λ , it turns out that the zeroth order is trivially fulfilled. In the first order, this yields:

$$\omega_n^{(1)} V_n + \omega_n \int_V dV \mathbb{F}_n^\dagger \cdot \delta\hat{\mathbb{P}}(\omega_n) \mathbb{F}_n = -S_n^{(1)}. \quad (103)$$

Here, V_n is the volume term of the normalization defined in equation (37). For the sake of brevity of notations, we have furthermore introduced the abbreviation:

$$S_n^{(1)} = ic \oint_{\partial V} d\mathbf{S} \cdot [\mathbf{E}_n^\dagger \times \mathbf{H}_n^{(1)} - \mathbf{E}_n^{(1)} \times \mathbf{H}_n^\dagger], \quad (104)$$

which closely resembles the surface term of the normalization given by equation (38). However, we should in this case replace $(\omega - \omega_n)S_n$ in equation (40) by $-\Lambda\omega_n\delta\hat{\mathbb{P}}(\omega_n)$, use equation (8) with the background Green's dyadic $\hat{\mathbb{G}}_0$, and sort by powers of Λ , which allows us to express the first-order correction as:

$$\mathbb{F}_n^{(1)} = \omega_n^{(1)}\mathbb{F}_n' - \frac{\omega_n}{c} \int dV \hat{\mathbb{G}}_0 \delta\hat{\mathbb{P}}(\omega_n)\mathbb{F}_n. \quad (105)$$

Thus, we obtain the frequency shift and linewidth change for sensing applications, which is given by the real and imaginary parts, respectively, of the first-order correction of the eigenfrequency as [14]:

$$\omega_n^{(1)} = - \frac{\omega_n \int dV \mathbb{F}_n^\dagger \cdot \delta\hat{\mathbb{P}}(\omega_n)\mathbb{F}_n + \delta S_n}{V_n + S_n}. \quad (106)$$

The denominator equals unity in the case of normalized RS, and we have introduced:

$$\delta S_n = ic \oint_{\partial V} d\mathbf{S} \cdot [\mathbf{E}_n^\dagger \times \delta\mathbf{H}_n - \delta\mathbf{E}_n \times \mathbf{H}_n^\dagger], \quad (107)$$

which equals zero in the case of perturbations localized to the resonator [11, 12]. Equation (107) contains the abbreviations $\delta\mathbf{E}$ and $\delta\mathbf{H}$ for the corrections of the electric and magnetic fields respectively, which are defined as elements of the super-vector:

$$\delta\mathbb{F}_n = - \frac{\omega_n}{c} \int dV \hat{\mathbb{G}}_0 \delta\hat{\mathbb{P}}(\omega_n)\mathbb{F}_n. \quad (108)$$

In the case that the perturbation is localized, the surface term δS_n in the numerator of equation (106) vanishes due to equation (27), because it results in purely outgoing fields. An alternative derivation for localized perturbations can be found in [26], additionally accounting for some corrections of the local fields.

If the perturbation is not localized, but homogeneous and isotropic in the surrounding, we can make the same analytic continuation for the fields in the exterior as described in section 2.3, see equation (45). However, the basis functions \mathbb{O}_N now explicitly depend on the perturbation parameter Λ , which allows us to calculate the related field correction as [14]:

$$\delta\mathbb{F}_n = \sum_N \alpha_N^{(n)}(\omega_n; \Lambda) \left. \frac{\partial \mathbb{O}_N(\mathbf{r}; \omega_n; \Lambda)}{\partial \Lambda} \right|_{\Lambda=0}, \quad (109)$$

where $\alpha_N^{(n)}$ is the same as in equation (46). In the simple case that the perturbation in the surrounding is given by scalar

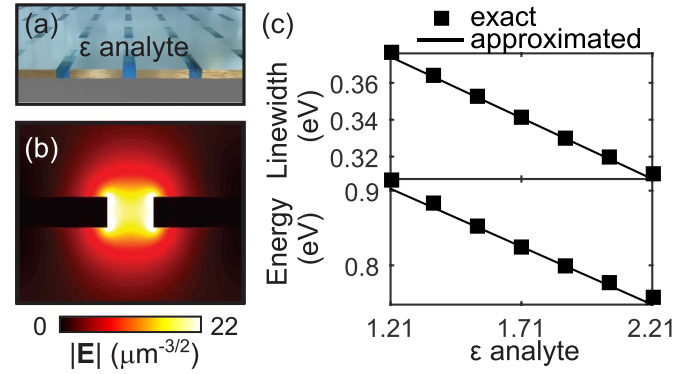


Figure 7. Perturbation theory applied to an array of plasmonic nanoslits. Panel (a) depicts the geometry: The structure consists of a gold layer, with the slits etched into it. The gold is sitting on a glass substrate and is covered by an analyte solution. As a perturbation, the permittivity of the analyte is changed. The electric-field intensity of the fundamental plasmon mode is displayed in (b). Panel (c) shows the resonance linewidth and energy of this mode as a function of the analyte's permittivity. The lines denote the results of the perturbation theory, while the squares correspond to numerically exact calculations. Adapted with permission from [14] © The Optical Society.

values $\delta\varepsilon$ and $\delta\mu$, the surface correction in equation (106) can then be rewritten as [14]:

$$\delta S_n = \frac{\eta\omega_n}{2} \left(\frac{\delta\varepsilon}{\varepsilon} + \frac{\delta\mu}{\mu} \right) S_n + \frac{i\eta\beta c}{2} \oint_{\partial V} d\mathbf{S} \cdot (\mathbf{E}_n^\dagger \times \mathbf{H}_n), \quad (110)$$

where ε and μ are the unperturbed values of permittivity and permeability, respectively, $\eta = \sqrt{\varepsilon\mu}/(\omega\sqrt{\varepsilon\mu})'$, and $\beta = [(\omega\mu)' \delta\varepsilon - (\omega\varepsilon)' \delta\mu]/\varepsilon\mu$. Here, the prime denotes again the derivative with respect to ω at ω_n , as introduced in section 2.3. For non-dispersive ε and μ , the above abbreviations simplify to $\eta = 1$ and $\beta = \delta\varepsilon/\varepsilon - \delta\mu/\mu$. It should be mentioned that it is also possible to treat homogeneous and isotropic perturbations of the surrounding medium beyond the above first-order approximation by using an adaption of the resonant-state expansion, in which the perturbation is mapped onto effective modifications in the system's interior [159].

Figure 7 displays an example, where the perturbation theory is applied to an array of plasmonic nanoslits. The example is taken from [14]. The geometry is depicted in panel (a): The system consists of a gold layer (height 40 nm, permittivity from [160]), with the slits etched into it. The gold is sitting on top of a glass substrate ($n = 1.5$) and is covered by an analyte solution. The slits are $60 \times 400 \text{ nm}^2$ in size and periodically arranged with periods of 300 nm and 700 nm, respectively. As a perturbation, the permittivity of the analyte is varied from its initial value of 1.71. The electric-field intensity of the fundamental plasmonic mode is displayed in panel (b). Panel (c) shows the linewidth and energy of this mode as a function of the analyte's permittivity. The lines denote the results of the perturbation theory (i.e. equation (106)), while the squares have been derived from numerically exact calculations. It is

evident that there is an excellent agreement over the large range of permittivity changes.

In sensor designs, it is often useful to quantify the sensing capability of an individual resonant state with respect to frequency shifts. For this purpose, it is very convenient to introduce the following figure of merit (FOM) [27]:

$$\text{FOM} = \frac{[\text{sensitivity}] \times [\text{excitation strength}]}{[\text{resonance linewidth}]}. \quad (111)$$

The quantities in this equation can be derived from the resonant state: the sensitivity is usually defined around the eigenfrequency $\omega_n = \Omega_n - i\Gamma_n$ as $|\text{Re}(\partial\omega_n/\partial X)|$, where X represents the material parameter that is varied. This expression can directly be evaluated from equation (106). The linewidth is known as $-2\Gamma_n$, and the excitation strength can be estimated as $|b_{\mathbf{N}}^{(n)}(\Omega_n)|$ from equation (77). In [27] it is demonstrated and experimentally verified how this figure of merit can be used to optimize the geometry of a complex sensor.

So far, only the effect of the perturbation on the eigenfrequencies was considered rigorously. Let us now investigate the influence of the perturbation on the scattering matrix for local perturbations. We will see that, besides frequency shifts and linewidth changes, there can occur further perturbation-induced effects, that also may lead to observable signals. We start from the total field $\mathbb{F}_{\text{tot}}^{\text{pert}}$ in the perturbed resonator. In analogy to equation (99), which describes RS of the perturbed resonator, the total field is defined via:

$$\left[\hat{\mathbb{M}}_0(\mathbf{r}; \omega) + \Lambda \frac{\omega}{c} \delta \hat{\mathbb{P}}(\mathbf{r}; \omega) \right] \mathbb{F}_{\text{tot}}^{\text{pert}}(\omega) = 0. \quad (112)$$

We write $\mathbb{F}_{\text{tot}}^{\text{pert}}$ as Taylor series in Λ and note that only the scattered field is affected by the perturbation, while the background field remains unaffected. This yields:

$$\mathbb{F}_{\text{tot}}^{\text{pert}} = \mathbb{F}_{\text{BG}} + \mathbb{F}_{\text{scat}} + \Lambda \mathbb{F}_{\text{scat}}^{(1)} + \Lambda^2 \mathbb{F}_{\text{scat}}^{(2)} + \dots, \quad (113)$$

where \mathbb{F}_{BG} and \mathbb{F}_{scat} denote the background and scattered field, respectively, in the unperturbed resonator, and $\mathbb{F}_{\text{scat}}^{(1)}$, $\mathbb{F}_{\text{scat}}^{(2)}$, ... are correction terms. Inserting equation (113) into equation (112) and comparing the coefficients for every power of Λ provides:

$$\hat{\mathbb{M}}_0 \mathbb{F}_{\text{scat}} = -\hat{\mathbb{M}}_0 \mathbb{F}_{\text{BG}} \quad (114)$$

$$\hat{\mathbb{M}}_0 \mathbb{F}_{\text{scat}}^{(1)} = -\frac{\omega}{c} \delta \hat{\mathbb{P}} \mathbb{F}_{\text{BG}} - \frac{\omega}{c} \delta \hat{\mathbb{P}} \mathbb{F}_{\text{scat}} \quad (115)$$

...

This set of equations implicitly describes the scattered field and all its correction terms. The first equation defines \mathbb{F}_{scat} and translates into the already known equation (52). The second equation defines the first-order correction term $\mathbb{F}_{\text{scat}}^{(1)}$. We can

solve it with the help of the Green's dyadic of the unperturbed system, which results in:

$$\begin{aligned} \mathbb{F}_{\text{scat}}^{(1)}(\omega) = & - \sum_n \mathbb{F}_n \frac{\omega \int dV \mathbb{F}_n^\dagger \cdot \delta \hat{\mathbb{P}}(\omega) \mathbb{F}_{\text{BG}}(\omega)}{\omega - \omega_n} \\ & - \sum_n \mathbb{F}_n \frac{\omega \int dV \mathbb{F}_n^\dagger \cdot \delta \hat{\mathbb{P}}(\omega) \mathbb{F}_{\text{scat}}(\omega)}{\omega - \omega_n}. \end{aligned} \quad (116)$$

Successively applying this method would allow for deriving expressions for all higher-order correction terms $\mathbb{F}_{\text{scat}}^{(2)}, \dots$; however, since the perturbation is assumed to be small, we do only need to consider the first order. Consequently, we write $\mathbb{F}_{\text{tot}}^{\text{pert}} \approx \mathbb{F}_{\text{BG}} + \mathbb{F}_{\text{scat}} + \mathbb{F}_{\text{scat}}^{(1)}$.

Let us now evaluate the scattering matrix of the perturbed system. In analogy to the calculation of the unperturbed scattering matrix (see equations (71) and (72)), we assume that the system gets excited via $\mathbb{I}_{\mathbf{N}}(\omega)$. This results in the total field $\mathbb{F}_{\text{tot},\mathbf{N}}^{\text{pert}} \approx \mathbb{F}_{\text{BG},\mathbf{N}} + \mathbb{F}_{\text{scat}} + \mathbb{F}_{\text{scat},\mathbf{N}}^{(1)}$. The scattering matrix is then obtained by projecting this total field onto the probe function $\mathbb{I}_{\mathbf{M}}^\dagger(\omega)$ via equation (69). One then obtains:

$$S_{\text{MN}}^{\text{pert}}(\omega) = S_{\text{MN}}(\omega) + \delta S_{\text{MN}}(\omega), \quad (117)$$

where S_{MN} denotes the scattering matrix of the unperturbed system, and δS_{MN} describes the perturbation-induced change:

$$\begin{aligned} \delta S_{\text{MN}}(\omega) = & i \oint_{\partial V} d\mathbf{S} \cdot \left[\mathbf{E}_{\text{in},\mathbf{M}}^\dagger(\omega) \times \mathbf{H}_{\text{scat},\mathbf{N}}^{(1)}(\omega) \right. \\ & \left. - \mathbf{E}_{\text{scat},\mathbf{N}}^{(1)}(\omega) \times \mathbf{H}_{\text{in},\mathbf{M}}^\dagger(\omega) \right]. \end{aligned} \quad (118)$$

To evaluate this term, we apply a similar procedure as it was used above to derive the symmetric representation of the unperturbed scattering matrix (i.e. equation (79)). First, we replace the basis function $\mathbb{I}_{\mathbf{M}}^\dagger$ with the corresponding background field $\mathbb{F}_{\text{BG},\mathbf{M}}^\dagger$. This is possible due to analog reasons as explained in section 2.7. Then, we use equation (22) to convert the surface integral into a volume integral, and after some algebra [138], we obtain:

$$\begin{aligned} \delta S_{\text{MN}}(\omega) = & -\frac{\omega}{c} \int dV \mathbb{F}_{\text{BG},\mathbf{M}}^\dagger(\omega) \cdot \delta \hat{\mathbb{P}}(\omega) \mathbb{F}_{\text{BG},\mathbf{N}}(\omega) \\ & -\frac{\omega}{c} \int dV \mathbb{F}_{\text{BG},\mathbf{M}}^\dagger(\omega) \cdot \delta \hat{\mathbb{P}}(\omega) \mathbb{F}_{\text{scat},\mathbf{N}}(\omega) \\ & -\frac{\omega}{c} \int dV \mathbb{F}_{\text{BG},\mathbf{M}}^\dagger(\omega) \cdot \Delta \hat{\mathbb{P}}_0(\omega) \mathbb{F}_{\text{scat},\mathbf{N}}^{(1)}(\omega). \end{aligned} \quad (119)$$

Finally, we insert the expansions of \mathbb{F}_{scat} and $\mathbb{F}_{\text{scat}}^{(1)}$ (given by equations (59) and (116), respectively), and utilize the definitions of $a_{\mathbf{M}}^{(n)}$ and $b_{\mathbf{N}}^{(n)}$ (given by equations (81) and (77), respectively). This gives the change of the scattering matrix as [138]:

$$\delta S_{\text{MN}} = \delta S_{\text{MN}}^{\text{nr}} + \delta S_{\text{MN}}^{\text{ex}} + \delta S_{\text{MN}}^{\text{em}} + \delta S_{\text{MN}}^{\text{shift}} + \delta S_{\text{MN}}^{\text{cross}}, \quad (120)$$

which consists of the following five contributions:

$$\delta S_{\text{MN}}^{\text{nr}}(\omega) = -\frac{\omega}{c} \int dV \mathbf{F}_{\text{BG},\text{M}}^\dagger(\omega) \cdot \delta \hat{\mathbb{P}}(\omega) \mathbf{F}_{\text{BG},\text{N}}(\omega) \quad (121)$$

$$\delta S_{\text{MN}}^{\text{ex}}(\omega) = \omega \sum_n \frac{a_{\text{M}}^{(n)}(\omega) \int dV \mathbf{F}_n^\dagger \cdot \delta \hat{\mathbb{P}}(\omega) \mathbf{F}_{\text{BG},\text{N}}(\omega)}{\omega - \omega_n} \quad (122)$$

$$\delta S_{\text{MN}}^{\text{em}}(\omega) = \omega \sum_n \frac{b_{\text{N}}^{(n)}(\omega) \int dV \mathbf{F}_{\text{BG},\text{M}}^\dagger(\omega) \cdot \delta \hat{\mathbb{P}}(\omega) \mathbf{F}_n}{\omega - \omega_n} \quad (123)$$

$$\delta S_{\text{MN}}^{\text{shift}}(\omega) = -\omega c \sum_n \frac{a_{\text{M}}^{(n)}(\omega) b_{\text{N}}^{(n)}(\omega) \int dV \mathbf{F}_n^\dagger \cdot \delta \hat{\mathbb{P}}(\omega) \mathbf{F}_n}{(\omega - \omega_n)^2} \quad (124)$$

$$\delta S_{\text{MN}}^{\text{cross}}(\omega) = -\omega c \sum_{n \neq m} \frac{a_{\text{M}}^{(n)}(\omega) b_{\text{N}}^{(m)}(\omega) \int dV \mathbf{F}_n^\dagger \cdot \delta \hat{\mathbb{P}}(\omega) \mathbf{F}_m}{(\omega - \omega_n)(\omega - \omega_m)} \quad (125)$$

Equations (120)–(125) allow to predict the change of the scattering matrix via simple overlap integrals over the unperturbed fields. Each of the five contributions describes the effect of a different perturbation-induced process onto the scattering matrix. The first one, $\delta S_{\text{MN}}^{\text{nr}}$, contains the overlap between the incoming and outgoing background fields and can be interpreted as a nonresonant background interaction. The second and third one, $\delta S_{\text{MN}}^{\text{ex}}$ and $\delta S_{\text{MN}}^{\text{em}}$, respectively, encompass overlap integrals between the background fields and the RS, and denote changes in the excitation and emission coefficients, respectively. The fourth one, $\delta S_{\text{MN}}^{\text{shift}}$, contains overlap integrals of the RS with themselves, which can be associated with their resonance frequency shifts for normalized fields and localized perturbations, see equation (106). The fifth one, $\delta S_{\text{MN}}^{\text{cross}}$, involves overlaps between different RS and accounts for perturbation-induced crosstalk.

The predictions of the first-order perturbation theory are demonstrated in figure 8 for the example of an array of gold antennas with a length of 150 nm, a width and height of 40 nm, and a periodicity of 650 nm. The top and bottom layers are infinite half spaces of vacuum, while the layer with the antennas contains cubic patches that are filled by water with a refractive index of $n = 1.33$. The spectra and a schematic of that system can be seen in figure 8(a). Exactly the same system is used in [161], but for changing the material in cubic patches at the end of the antennas from achiral to chiral. Here, we consider a change of permittivity in the cubic patches, which is 0.0001. The resulting transmittance changes can be seen in figure 8(b). The red dots represent numerical results, while the gray shaded area denotes the prediction from the first-order perturbation theory for a single resonant state at 1591–45i meV. Additionally, we analyze the different contributions, which correspond to the resonance shift (red solid line), the changes in the excitation and emission coefficients (blue dashed line), and the nonresonant background interaction (black dotted line). Evidently, the dominant contribution stems from the resonance shift—in contrast to chiral systems, where the resonance shift does not contribute at all for such achiral geometries [138].

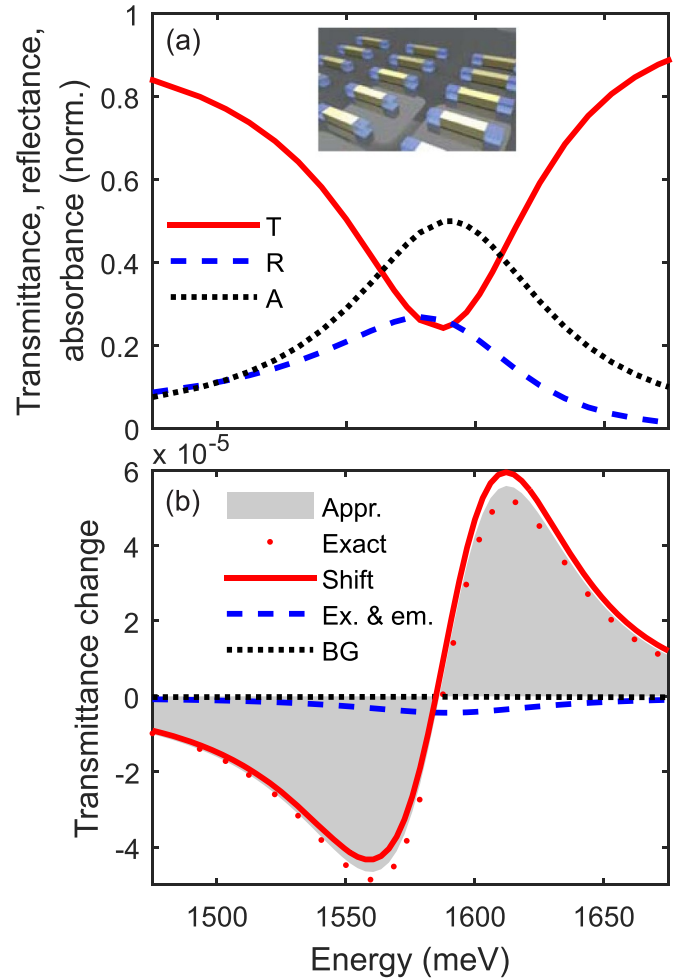


Figure 8. Perturbation theory for rod antenna array: The permittivity is changed in the blue regions at the end of gold antennas (schematic in inset) by 0.0001. Panel (a) displays the transmittance (red), reflectance (blue), and absorbance (black) at normal incidence. The change in transmittance is shown in panel (b), with red dots denoting exact numerical results. The gray-shaded area denotes the approximated results obtained by first-order perturbation theory using equations (117) and (120). Furthermore, we plot the individual contributions to the transmittance change: resonance shift (red solid line), excitation and emission change (blue dashed line) and nonresonant background interaction (black dotted line).

3.3. Purcell enhancement

Countless applications in micro- and nanophotonics [43, 122, 162–171] exploit the interaction of dipole emitters with resonators. The heart of this interaction is the so-called Purcell effect, which describes the enhancement of the spontaneous emission rate that an emitter experiences when being coupled to a resonator. In his famous 1946 communication [172], Purcell stated that this enhancement is given as:

$$F = \frac{6\pi c^3 Q_n}{\omega^3 V_n}, \quad (126)$$

which is nowadays known as the Purcell factor. Here, ω denotes the dipole's oscillation frequency, $Q_n = \Omega_n/2\Gamma_n$ is the

quality factor of the optical mode, and V_n represents the mode volume. Initially, V_n was estimated as the effective volume of the resonator. Later, this definition was refined to (see for instance [7, 173, 174]):

$$V_n = \frac{\int dV \varepsilon(\mathbf{r}) |\mathbf{E}_n(\mathbf{r})|^2}{|\mathbf{e}_d \cdot \mathbf{E}_n(\mathbf{r}_d)|^2}, \quad (127)$$

where \mathbf{E}_n represents the modal field, \mathbf{e}_d describes the unit vector along the dipole orientation, \mathbf{r}_d represents the dipole position, and the integration is carried out over the volume occupied by the mode. Note that in consistency with [7], we reference the Purcell factor to the spontaneous emission rate in vacuum instead of a bulk medium, as it is also common in literature. The equations for a bulk medium can be obtained by simply including factors of $1/n^3$ and $1/n^2$ in the definition of F and V_n , respectively, where n represents the bulk's refractive index.

Although equations (126) and (127) have been used for decades to describe light-matter interactions, it turns out that they are correct only in the limit of high quality factors and negligible energy leakage to the environment. The main reason is that—as discussed in subsection 2.3—in the case of energy leakage, the modal field distributions become exponentially growing with distance to the resonator and the integral in equation (127) is not applicable anymore. A first solution was suggested by Kristensen *et al* [2], where they introduced a generalized mode volume, based on an extension of a normalization scheme for open resonators that had been developed in the 1990s by Leung *et al* [175–177]. However, while this approach was aiming in the right direction, it was later shown that the normalization used in [2] has a mathematical flaw (for details, see literature debate in [7, 18, 89, 90, 92, 93]). Furthermore, this initial work focused on the case of an emitter interacting with only one single mode and being spectrally matched with this one. The first correct and rigorous theory was presented by Sauvan *et al* [3], based on the normalization via equation (35) using perfectly-matched layers and an orthogonality decomposition of the fields inside the resonator in terms of RS (for an explanation, see section 2.4). Shortly after, the first fully analytical treatment—similar to Sauvan's approach, but based on the analytic mode normalization and the analytic pole expansion of the Green's dyadic—was developed by Muljarov and Langbein [7]. In the following, we present the generalization of Purcell's theory to open systems, following mostly the derivation from this latter work. Note that we remain here in the weak-coupling regime between emitter and resonator, where the RS are still classical quantities. However, it has been shown by Franke *et al* that it is possible to quantize the RS for describing the interaction of resonator and emitter on the few-photon level in a quantum-mechanical framework [178].

As shown in [2, 3, 7, 10, 18, 94, 179, 180], the correct Purcell factor for open electromagnetic resonators becomes:

$$F(\omega) = \frac{3\pi c^3}{\omega} \sum_n \text{Im} \frac{1}{V_n \omega_n (\omega_n - \omega)}, \quad (128)$$

with the generalized mode volume V_n defined as:

$$V_n = \frac{1}{2[\mathbf{e}_d \cdot \mathbf{E}_n^\dagger(\mathbf{r}_d)][\mathbf{e}_d \cdot \mathbf{E}_n(\mathbf{r}_d)]}, \quad (129)$$

where \mathbf{E}_n and \mathbf{E}_n^\dagger are normalized according to equations (36)–(38) or an equivalently applicable method [1, 3, 5, 88, 93]. Note that in comparison to [7], we have included a factor of 2 in order to be consistent with the normalization used in this review (which is defined via electric and magnetic fields instead of electric fields only), and furthermore generalized to the case where $\mathbf{E}_n^\dagger \neq \mathbf{E}_n$.

It can be shown easily that the original Purcell factor of equation (126) is contained in equation (128) in the limit of high quality factors and negligible energy leakage. An important aspect of the generalized mode volume is that it can be complex [2, 3, 6, 94, 180], in contrast to its original definition, in which it is a real-valued positive number. This has two remarkable consequences (for a detailed discussion, see [3, 94]): first, modes with $\text{Im}(V_n) \neq 0$ contribute with non-Lorentzian features to the spectral dependence of $F(\omega)$. Second, modes with $\text{Re}(V_n) < 0$ provide a negative contribution to the overall enhancement.

Let us have a short excursion about the physical meaning of the Purcell factor. There are three different viewpoints [181], which can be summarized as:

$$F \stackrel{\text{(i)}}{=} \frac{\gamma}{\gamma_0} \stackrel{\text{(ii)}}{=} \frac{\rho}{\rho_0} \stackrel{\text{(iii)}}{=} \frac{P}{P_0}. \quad (130)$$

Viewpoint (i) resembles the definition mentioned at the beginning of this section, according to which F expresses the enhancement of the spontaneous emission rate γ of a dipole interacting with the resonator compared to its spontaneous emission rate γ_0 in vacuum. As stated by Fermi's golden rule [181], the spontaneous emission rate is proportional to the partial local density of states. Consequently, viewpoint (ii) denotes F as the increase of this density, where ρ represents the value in the presence of the resonator, and ρ_0 is the vacuum value. This concept is especially useful when dealing with systems that contain a multitude of emitters, as it is for example the case in [168, 169]. Concerning the physical interpretation of ρ in open resonators, one needs, however, to be careful: in closed cavities, the density of states can be understood as the number of available electromagnetic modes per frequency interval $d\omega$, in analogy to the electronic density of states in solid-state physics. (The distinction between the density of states and the partial local density of states simply stems from the fact that the latter one contains an additional weighting factor that accounts for the coupling to the emitter [94].) In open resonators, the above interpretation breaks down. Intuitively, we can understand this from the fact that the modes of open resonators (i.e. the resonant states) have in general non-negligible linewidths and can spectrally interfere with each other. A detailed explanation of this matter is found in [94]. In this general case, the appropriate interpretation of ρ/ρ_0 is to associate it with the resonator-induced change of the local electric field generated by the emitter. Closely related is viewpoint (iii), which describes F as the enhancement of the power

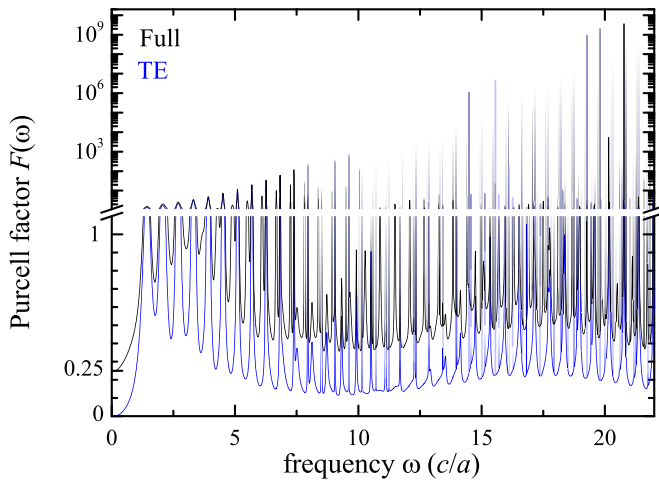


Figure 9. Purcell factor inside a dielectric sphere. The sphere has a radius of a and a permittivity of $\varepsilon = 4$. The emitter is placed at a distance of $0.9a$ from the center and the Purcell factor is averaged over the polarization directions. The black line displays the full Purcell factor, while the blue line denotes the partial Purcell factor, considering only transverse-electric (TE) modes. Reprinted figure with permission from [7], Copyright (2016) by the American Physical Society.

P that is radiated by a classical dipole in the presence of the resonator compared to the power P_0 that the same dipole would radiate in vacuum.

An example for the Purcell factor calculation in an open resonator is shown in figure 9, which is taken from [7]. Plotted is $F(\omega)$ for a dielectric sphere with radius a and the permittivity $\varepsilon = 4$, which is surrounded by air. The emitter is assumed to be located at a distance of $0.9a$ from the center. The Purcell factor is calculated via equation (128), taking into account modes with an angular quantum number of $l < 38$ and eigenfrequencies $|\omega_n| < 40c/a$, and is averaged over the polarization directions. The black line represents the full Purcell factor, while the blue line corresponds the partial Purcell factor, considering only transverse-electric (TE) modes.

It should be mentioned, that—due to the completeness issue discussed in section 2.6—the decomposition of the Purcell factor in terms of the resonant state is strictly speaking only valid inside the resonator. Yet, in practise, reasonably accurate predictions are also obtained for dipoles placed outside in the vicinity of the resonator [3, 4, 18, 95]. Even at intermediate distances, the above decomposition might still deliver correct results when the coupling to the free-space continuum is accounted for via adding an additional factor [3, 4, 18] (in the case of air this factor is 1). However, at long distances, namely when the exponential growth of the RS starts to dominate, even this extended approach is condemned to fail and will predict unphysically high-values of $F(\omega)$. The problem can be circumvented using one of the following two methods: the first option consists in calculating a mapped system, where the resonator and its surrounding are enclosed by perfectly-matched layers, and include the non-physical perfectly-matched layer modes in the expansion [10]. This ensures completeness in the whole calculation domain. The second option is to use a

regularization of the modal fields in the exterior of the resonator to remove the exponential growth [4, 182] (note, however, that [4] uses the same normalization as [2], but can be also extended to other normalization methods).

At the end, let us have a closer look at the complex mode volume. One might think that this is purely an abstract mathematical construct, only meaningful because it appears in the Purcell factor calculation. However, it turns out that V_n itself is an observable quantity. It was predicted by Yang *et al* [26] that when a tiny electrically polarizable object is placed inside (or nearby) an optical resonator, the complex eigenfrequency ω_n of the resonator's mode experiences a change that is approximately proportional to the value of $1/V_n$ at the object's position. Hence, by probing the real and imaginary part of this eigenfrequency change (recall that they are measurable via the shift in the resonance frequency and the change in linewidth, respectively), one can experimentally access the complex nature of V_n . Such an experiment was completed by Cognée *et al* [19]. By moving the electrically polarizable tip of a scanning near-field optical microscope over a photonic crystal cavity and simultaneously recording the peak frequency and the linewidth of the cavity's fluorescence spectrum, they were able to construct a spatially resolved map of the cavity's inverse complex mode volume. The results are displayed in figure 1(d). The left and right plots correspond to the real and imaginary part, respectively. It is evident that the experimental data (top) coincides very well with their numerical predictions (bottom). Recently, this approach was extended to magnetic mode volumes, i.e. the magnetic analog of equation (129) [183]. The experimental observation of complex mode volumes constitutes an important example where the theory of RS has led to the prediction and discovery of a new phenomenon. This clearly demonstrates that the theory is much more than only a computational tool.

4. Related topics

4.1. Permittivity eigenmodes

While the expansion of optical properties in terms of RS is based on an analytic continuation of this response to the complex frequency plane, other forms of analytic continuation are possible, too. One highly relevant case is that of an analytic continuation to a complex permittivity plane for a fixed real-valued frequency. The basic idea originates in electrostatics [184, 185] and has been later extended to electrodynamics [186, 187].

The starting point is the wave equation for non-magnetic materials ($\mu = 1$), which is:

$$\nabla \times \nabla \times \mathbf{E} - \frac{\omega^2}{c^2} \varepsilon(\mathbf{r}; \omega) \mathbf{E} = i \frac{4\pi\omega}{c^2} \mathbf{j}. \quad (131)$$

As in section 2.5, we separate the permittivity into a background part ε_{BG} , which is now assumed to be homogeneous and isotropic, and the scattering geometry, which is given by $\Delta\varepsilon = (\varepsilon - \varepsilon_{\text{BG}})\Theta(\mathbf{r})$, where Θ is a Heaviside function that is one inside and zero outside the scattering geometry. Using the

well-known analytic form for the Green's dyadic \hat{G}_0 of the background material [188], which satisfies:

$$\left(\nabla \times \nabla \times - \frac{\omega^2}{c^2} \varepsilon_{\text{BG}}\right) \hat{G}_0(\mathbf{r}, \mathbf{r}'; \omega) = \hat{I} \delta(\mathbf{r} - \mathbf{r}'), \quad (132)$$

where \hat{I} is a 3×3 unit matrix, it is possible to set up the following eigenvalue equation for $\mathbf{j} = 0$ [189]:

$$s_m \mathbf{E}_m(\mathbf{r}) = -\varepsilon_{\text{BG}} \frac{\omega^2}{c^2} \int dV' \hat{G}_0(\mathbf{r}, \mathbf{r}'; \omega) \Theta(\mathbf{r}') \mathbf{E}_m(\mathbf{r}). \quad (133)$$

Here, s_m is the Bergman spectral parameter:

$$s_m = \frac{\varepsilon_{\text{BG}}}{\varepsilon_{\text{BG}} - \varepsilon_m}, \quad (134)$$

with ε_m as the eigenpermittivity and \mathbf{E}_m as the corresponding eigenfield. Then, all relevant quantities can be expanded in terms of these permittivity eigenmodes. A general description of such expansions can be found in [189–191].

The huge advantage of the permittivity eigenmodes is that they constitute a complete basis set, which holds not only inside the scattering geometry, but over the entire space, and the related eigenfields do not diverge in the exterior. Hence, there are no problems in field expansions outside the scattering geometry, e.g. in the case of an emitter in the exterior. There is also no need to find an analytic continuation of the material parameters to the complex frequency plane, because the method considers only real frequencies, where experimental data is available for material parameters such as the permittivity. Furthermore, it is possible to describe the coupling of two or more scattering geometries in a mode-hybridization theory [192], which yields a simple linear eigenvalue problem for the coupling of the individual resonators. Attempts of setting up a coupled-mode theory via RS either suffer from inaccuracies in the far-field coupling [193–197] or involve a nonlinear eigenvalue problem [95, 198]. For the simple case of stacked gratings, however, an extended linear eigenvalue problem for the RS is developed in [199].

The downside of the permittivity eigenmodes is that an expansion of any optical properties in terms of these modes has to be repeated for each frequency of interest. Also, it is more difficult to grasp the physical meaning of the complex eigenpermittivity and the related eigenfields. Finally, the question arises about how to deal with several different materials, because the classical formulation only includes a background permittivity and the permittivity of the scattering geometry.

4.2. Propagating modes

In the case that the system of interest exhibits a certain translational symmetry, the complexity of that system can be mathematically reduced from a three-dimensional problem to a two-dimensional problem, see [200] and references therein. This can be achieved formally by carrying out a Fourier transform in the direction of translational symmetry. For instance, an ideal fiber or waveguide may be invariant under translations

along the z direction. Then, we can apply the Fourier transform:

$$\tilde{f}(x, y; \beta) = \frac{1}{2\pi} \int dz e^{-i\beta z} f(x, y, z), \quad (135)$$

which transforms Maxwell's equations from equation (2) to:

$$\tilde{\mathbb{M}}(x, y; \beta; \omega) \tilde{\mathbb{F}}(x, y; \beta; \omega) = \tilde{\mathbb{J}}(x, y; \beta; \omega), \quad (136)$$

where $\tilde{\mathbb{M}}$ originates from the Maxwell operator $\hat{\mathbb{M}}$ in equation (2) by the substitution $\partial_z \rightarrow i\beta$ [84]. Historically, this Fourier transformation is mostly applied to the wave equation [201].

Fixing the frequency to a real value, we can then make an analytic continuation of equation (136) to the complex β plane. The related Green's dyadic $\tilde{\mathbb{G}}$ exhibits poles at complex β values, which we can relate to so-called propagating modes that obey the following constitutive equation with outgoing boundary conditions:

$$\tilde{\mathbb{M}}(x, y; \beta_n; \omega) \tilde{\mathbb{F}}_n(x, y; \omega) = 0. \quad (137)$$

As in the case of RS, it is then possible to expand the optical response in the basis of these propagating modes. From a physical perspective, propagating modes constitute solutions of Maxwell's equations in real space with a field distribution:

$$\mathbb{F}_n(x, y, z; \omega) = \tilde{\mathbb{F}}_n(x, y; \omega) e^{i\beta_n z}, \quad (138)$$

which propagates along the z direction with only a change in phase that is governed by the real part of β_n and an exponential decay that stems from the imaginary part of β_n . In many cases, such as conventional step-index fibers [201], the dominant propagating modes exhibit a real-valued eigenvalue β_n , so that their fields are bound to a localized high-index region and decay perpendicular to the z axis with distance to this central region. These propagating modes are called 'bound modes,' with a normalization similar to equation (34). However, there are also solutions with a nonzero imaginary part of β_n that are called 'leaky modes,' because their fields grow perpendicular to the z axis with distance to the central region [81, 82, 201]. As discussed in section 2.3, similar normalization approaches as in equation (35) have been developed in the past [81, 82]. Only recently, the analytic normalization for RS from [91] has been adapted to these leaky modes and combined with the resonant-state expansion [83, 84]. Similarly, the first-order perturbation theory for homogeneous and isotropic perturbations in the exterior surrounding described in [14] has been transferred to leaky modes [102]. Based on this approach, it is possible to calculate the group velocity from the resonant field distributions when considering the frequency as global perturbation.

4.3. Application in nonlinear optics

In most derivations, the theory of RS relies on the use of reciprocal materials, see [84, 91, 94] and references therein. Reciprocity is a very fundamental principle that can be broken only

by a few possibilities [109]. One of them is based on nonlinearities. While we have shown here that the theory of RS can be extended to nonreciprocal materials, it still relies on the assumption of a linear material response. Hence, it might seem counterintuitive that it is possible to apply the theory of RS in nonlinear optics.

However, in the case of propagating modes, the description of nonlinear pulse propagation in optical fibers is mostly based on using a single or few bound modes as basis [202], resulting for a single mode with index m in the nonlinear Schrödinger equation:

$$\partial_z A_m \approx i\gamma |A_m|^2 A_m - i \frac{\bar{\beta}_m^{(2)}}{2} \partial_\tau^2 A_m - \bar{\alpha}_m^{(0)} A_m. \quad (139)$$

Here, A_m is the frequency-dependent amplitude of that modes, $\tau = t - \bar{\beta}_m^{(1)} z$, while $\bar{\beta}_m^{(n)}$ and $\bar{\alpha}_m^{(n)}$ are the n th order frequency derivatives of the real and imaginary parts of the propagation constant β_m (see previous section) at a central frequency ω_0 . Furthermore, γ is the Kerr nonlinearity parameter related to a third-order nonlinearity, which is typically calculated via an integral over expressions containing the correctly normalized modes [202].

The nonlinear Schrödinger equation is applicable, because the third-order nonlinearity is usually rather small, so that it is possible to treat it in a perturbative manner. In the case that we consider the propagation of leaky modes, it turns out that equation (139) remains valid, but the calculation of the Kerr nonlinearity parameter becomes more complicated due to the leakiness of the modes [113, 203–205]. Interestingly, γ is no longer real, but in general a complex number with the imaginary part resulting either in nonlinear loss or even nonlinear gain for the overall attenuating pulses [113]. The nonlinear gain results in optical pulses that are spectrally broader and more compressed temporally than expected from the simpler theory of bound modes. In addition to the Kerr nonlinearity, it is also possible to describe four-wave mixing of bound and leaky modes [114, 202].

While the nonlinear Schrödinger equation is a theoretical description of Kerr nonlinearities based on propagating modes, RS associated to poles of the Green's dyadic on the complex frequency plane have been used for approximating nonlinear responses, too. In the case of harmonic generation [206], the nonlinear susceptibility of order n generates fields at frequency $n\omega$. In the so-called undepleted pump approximation [207–209], the energy transfer from the pump frequency to the harmonic is neglected, which allows to first solve Maxwell's equations at the pump frequency and then to calculate the field emitted at the n th harmonic by considering the nonlinear polarization as an equivalent source current. The fields at the fundamental harmonic can be expanded in terms of the RS as described in section 2.5. Using the pole expansion of the Green's dyadic in equation (29) at the harmonic frequency, it is then possible to derive also the emitted field in the basis of RS [210].

In the case of the Kerr nonlinearity, it is not possible to neglect the interplay of the linear fields and the contributions due

to the nonlinear susceptibility. Still, it has been shown that one can use a modal description in terms of RS to approximate the Kerr nonlinearity in a ring resonator by appropriately accounting for the stored energy density [211].

5. Conclusion and outlook

We have shown here that the theory of RS follows directly from the analytic continuation of Maxwell's equations to the complex frequency plane. Thus, it is often possible to describe the optical response solely in terms of contributions from the discrete set of RS. More specifically, the Green's dyadic and related quantities such as the near and far field exhibit poles at the complex eigenfrequencies of the RS. The corresponding weight functions and residues of the poles can be associated to the resonant field distributions of the considered system and its transposed counterpart. Thus, the near and far field in a given frequency range can be often expanded by the pole contributions of a small set of relevant RS and a background contribution that summarizes distant poles and nonresonant terms. Care has to be taken, because the expansion in terms of RS is not complete in the exterior of the resonator structure, but possible workarounds have been discussed above.

When knowing a larger set of RS as basis for a reference system, we have summarized how to set up the resonant-state expansion, which is a perturbative method up to arbitrary orders of perturbations that yields the RS of a perturbed system as solutions of a simple eigenvalue equation. In general, this requires accounting for cut contributions and static modes. The first-order approximation of the resonant-state expansion results in simplified analytic expressions for resonance shifts and linewidth changes, which can be used for analyzing and optimizing nanoresonators for resonantly enhanced refractive-index sensors. Extensions to external perturbations as well as how to derive spectral changes in such sensors are provided here, too. Finally, we included an overview of how to describe the Purcell effect for open resonators based on the theory of RS.

However, the theory of RS has also some drawbacks, as mentioned above. Mostly, they are related to the growing nature of the RS outside the resonator geometry. Some of these issues can be resolved when switching to other modal methods, see section 4. Still, the question remains if the theory of RS is more than a complex mathematical approach to describe only simple resonant lineshapes.

In his book 'The Principles of Quantum Mechanics,' Paul Dirac states [212]: 'the only object of theoretical physics is to calculate results that can be compared with experiment. . . it is quite unnecessary that any satisfactory description of the whole course of the phenomena should be given.' Based on that, any reasonable numerical method would be just as good as a profound theory. However, it is also Dirac, who admits [213]: 'it is more important to have beauty in one's equations than to have them fit experiment.' Of course, it is difficult to quantify the beauty of a theory. Richard Feynman adds [214] that 'you can recognize truth by its beauty

and simplicity.’ A good theory should therefore be simple and agree with experimental observations. But besides being descriptive and explanatory, which is something that can be often afforded by numerical calculations, theory should be also predictive, i.e. one should be able to deduce new phenomena that can be later verified experimentally. Let us see how the theory of RS fits into these classifications of a good theory.

First, we have provided here several examples, where the theory of RS yields good agreement with experimental measurements [19, 27, 183, 198]. In fact, this list of theory-experiment collaboration is not complete, but it has to be admitted that so far, most publications on the theory of resonant states compare this theory with some sort of analytic or numerical results. Of course, by knowing that these numerical tools have predicted experimental observations accurately in the past, it is possible to deduce that the theory of resonant states will be able to achieve the same in the near future. Probably, such theory-experiment collaboration will be the major route for the theory of resonant states in this decade, with several recent publications from the Lalanne group pointing in that direction [183, 198].

In contrast to numerical schemes, the theory of resonant states describes optical properties in the physically-meaningful basis of resonant states, which gives further insight into the underlying physics [27, 138]. Even nonlinear phenomena can be considered in that way. Most importantly, the theory follows directly from Maxwell’s equations, so that all arising contributions can be calculated either analytically or numerically without the need to carry out any fitting procedures. This definitely proves the existence of beauty and generality in the theory of resonant states. The challenge is to derive all relevant resonant states for a given system. Once this is achieved, the optical properties of this system can be derived efficiently. Further analysis then allows optimizing the system for certain applications such as sensing.

However, the coexistence of several formulations for the expansion of the near and far fields is sort of unsatisfactory. The reason for this plethora of formulations may be the over-completeness of the resonant states. To resolve this issue, a thorough benchmarking of different approaches is preferable in the future. Nevertheless, the different formulations have proven to work well, and which formulation is superior may depend on the field of application.

Finally, there are examples, where the theory of resonant states has been predictive [19, 183]. This underlines the power of this theory beyond conventional numerical methods to solve Maxwell’s equations. Also, we would like to mention that concepts such as the resonant-state expansion can be applied to different fields in physics such as quantum mechanics [215], and even different disciplines can be married in a unifying theory, as shown for optomechanic systems [216].

Data availability statement

The data that support the findings of this study are available upon reasonable request from the authors.

Acknowledgments

We acknowledge support from the Deutsche Forschungsgemeinschaft (DFG) via the priority program SPP 1834 ‘Tailored disorder’ as well as the individual DFG research Grant No. WE 5815/5-1. Furthermore, we thank Ulrich Hohenester, Frank Neubrech, Martin Schäferling, and Josselin Defrance for their valuable input.

ORCID iDs

S Both  <https://orcid.org/0000-0002-2050-6952>

T Weiss  <https://orcid.org/0000-0002-4991-6779>

References

- [1] Muljarov E A, Langbein W and Zimmermann R 2010 Brillouin–Wigner perturbation theory in open electromagnetic systems *Europhys. Lett.* **92** 50010
- [2] Kristensen P T, Van Vlack C and Hughes S 2012 Generalized effective mode volume for leaky optical cavities *Opt. Lett.* **37** 1649–51
- [3] Sauvan C, Hugonin J P, Maksymov I S and Lalanne P 2013 Theory of the spontaneous optical emission of nanosize photonic and plasmon resonators *Phys. Rev. Lett.* **110** 237401
- [4] Ge R-C, Kristensen P T, Young J F and Hughes S 2014 Quasinormal mode approach to modelling light-emission and propagation in nanoplasmonics *New J. Phys.* **16** 113048
- [5] Doost M B, Langbein W and Muljarov E A 2014 Resonant-state expansion applied to three-dimensional open optical systems *Phys. Rev. A* **90** 013834
- [6] Muljarov E A and Langbein W 2016 Resonant-state expansion of dispersive open optical systems: creating gold from sand *Phys. Rev. B* **93** 075417
- [7] Muljarov E A and Langbein W 2016 Exact mode volume and Purcell factor of open optical systems *Phys. Rev. B* **94** 235438
- [8] Yang J, Hugonin J P and Lalanne P 2016 Near-to-far field transformations for radiative and guided waves *ACS Photonics* **3** 395–402
- [9] Lobanov S V, Langbein W and Muljarov E A 2018 Resonant-state expansion of three-dimensional open optical systems: light scattering *Phys. Rev. A* **98** 033820
- [10] Yan W, Faggiani R and Lalanne P 2018 Rigorous modal analysis of plasmonic nanoresonators *Phys. Rev. B* **97** 205422
- [11] Weiss T, Mesch M, Schäferling M, Giessen H, Langbein W and Muljarov E A 2016 From dark to bright: first-order perturbation theory with analytical mode normalization for plasmonic nanoantenna arrays applied to refractive index sensing *Phys. Rev. Lett.* **116** 237401
- [12] Weiss T, Schäferling M, Giessen H, Gippius N A, Tikhodeev S G, Langbein W and Muljarov E A 2017 Analytical normalization of resonant states in photonic crystal slabs and periodic arrays of nanoantennas at oblique incidence *Phys. Rev. B* **96** 045129
- [13] Weiss T and Muljarov E A 2018 How to calculate the pole expansion of the optical scattering matrix from the resonant states *Phys. Rev. B* **98** 085433
- [14] Both S and Weiss T 2019 First-order perturbation theory for changes in the surrounding of open optical resonators *Opt. Lett.* **44** 5917–20

- [15] Gras A, Yan W and Lalanne P 2019 Quasinormal-mode analysis of grating spectra at fixed incidence angles *Opt. Lett.* **44** 3494–7
- [16] Doost M B, Langbein W and Muljarov E A 2012 Resonant-state expansion applied to planar open optical systems *Phys. Rev. A* **85** 023835
- [17] Armitage L J, Doost M B, Langbein W and Muljarov E A 2014 Resonant-state expansion applied to planar waveguides *Phys. Rev. A* **89** 053832
- [18] Kristensen P T and Hughes S 2014 Modes and mode volumes of leaky optical cavities and plasmonic nanoresonators *ACS Photonics* **1** 2–10
- [19] Cognée K G, Yan W, La China F, Balestri D, Intonti F, Gurioli M, Koenderink A F and Lalanne P 2019 Mapping complex mode volumes with cavity perturbation theory *Optica* **6** 269–73
- [20] Tikhodeev S G, Muljarov E A, Langbein W, Gippius N A, Giessen H and Weiss T 2021 Influence of disorder on a Bragg microcavity *J. Opt. Soc. Am. B* **38** 139–50
- [21] Alpeggiani F, Parappurath N, Verhagen E and Kuipers L 2017 Quasinormal-mode expansion of the scattering matrix *Phys. Rev. X* **7** 021035
- [22] Zhang H and Miller O D 2020 Quasinormal coupled mode theory (arXiv:2010.08650 [physics.optics])
- [23] Benzaouia M, Joannopoulos J D, Johnson S G and Karalis A 2021 Quasi-normal mode theory of the scattering matrix, enforcing fundamental constraints for truncated expansions *Phys. Rev. Res.* **3** 033228
- [24] Wiersig J 2014 Enhancing the sensitivity of frequency and energy splitting detection by using exceptional points: application to microcavity sensors for single-particle detection *Phys. Rev. Lett.* **112** 203901
- [25] Zhang W and Martin O J F 2015 A universal law for plasmon resonance shift in biosensing *ACS Photonics* **2** 144–50
- [26] Yang J, Giessen H and Lalanne P 2015 Simple analytical expression for the peak-frequency shifts of plasmonic resonances for sensing *Nano Lett.* **15** 3439–44
- [27] Mesch M, Weiss T, Schäferling M, Hentschel M, Hegde R S and Giessen H 2018 Highly sensitive refractive index sensors with plasmonic nanoantennas—utilization of optimal spectral detuning of fano resonances *ACS Sens.* **3** 960–6
- [28] Louisell W H 1955 Analysis of the single tapered mode coupler *Bell Syst. Tech. J.* **34** 853–70
- [29] Maybee J S 1966 Normal and quasi-normal modes in damped linear dynamic systems *J. Appl. Mech.* **33** 413–6
- [30] Thorne K S and Campolattaro A 1967 Nonradial pulsation of general-relativistic stellar models. I. Analytic analysis for $l \geq 2$ *Astrophys. J.* **149** 591
- [31] Humblet J and Rosenfeld L 1961 Theory of nuclear reactions: I. Resonant states and collision matrix *Nucl. Phys.* **26** 529–78
- [32] Vollmer F and Arnold S 2008 Whispering-gallery-mode biosensing: label-free detection down to single molecules *Nat. Methods* **5** 591–6
- [33] Arnold S, Khoshsima M, Teraoka I, Holler S and Vollmer F 2003 Shift of whispering-gallery modes in microspheres by protein adsorption *Opt. Lett.* **28** 272–4
- [34] Toropov N, Cabello G, Serrano M P, Gutha R R, Rafti M and Vollmer F 2021 Review of biosensing with whispering-gallery mode lasers *Light Sci. Appl.* **10** 42
- [35] Barnes W L, Dereux A and Ebbesen T W 2003 Surface plasmon subwavelength optics *Nature* **424** 824–30
- [36] Stockman M I, Faleev S V and Bergman D J 2001 Localization versus delocalization of surface plasmons in nanosystems: can one state have both characteristics? *Phys. Rev. Lett.* **87** 167401–1–14
- [37] Podolskiy V, Sarychev A and Shalaev V 2003 Plasmon modes and negative refraction in metal nanowire composites *Opt. Express* **11** 735–45
- [38] Nordlander P, Oubre C, Prodan E, Li K and Stockman M I 2004 Plasmon hybridization in nanoparticle dimers *Nano Lett.* **4** 899–903
- [39] Murray W A and Barnes W L 2007 Plasmonic materials *Adv. Mater.* **19** 3771–82
- [40] McMahon J M, Henzie J, Odom T W, Schatz G C and Gray S K 2007 Tailoring the sensing capabilities of nanohole arrays in gold films with Rayleigh anomaly-surface plasmon polaritons *Opt. Express* **15** 18119–29
- [41] Mayer K M and Hafner J H 2011 Localized surface plasmon resonance sensors *Chem. Rev.* **111** 3828–57
- [42] Juan M L, Righini M and Quidant R 2011 Plasmon nano-optical tweezers *Nat. Phys.* **5** 349–56
- [43] Xin L *et al* 2019 Watching a single fluorophore molecule walk into a plasmonic hotspot *ACS Photonics* **6** 985–93
- [44] Yablonovitch E, Gmitter T J and Leung K M 1991 Photonic band structure: the face-centered-cubic case employing nonspherical atoms *Phys. Rev. Lett.* **67** 2295–8
- [45] Krauss T F, DeLaRue R M and Brand S 1996 Two-dimensional photonic-bandgap structures operating at near-infrared wavelengths *Nature* **383** 699–702
- [46] Russell P S J 2003 Photonic crystal fibers *Science* **299** 358–62
- [47] Staude I *et al* 2013 Tailoring directional scattering through magnetic and electric resonances in subwavelength silicon nanodisks *ACS Nano* **7** 7824–32
- [48] Eismann J, Neugebauer M and Banzer P 2018 Exciting a chiral dipole moment in an achiral nanostructure *Optica* **5** 954–9
- [49] Tzarouchis D and Sihvola A 2018 Light scattering by a dielectric sphere: perspectives on the Mie resonances *Appl. Sci.* **8** 184
- [50] Picardi M F, Neugebauer M, Eismann J S, Leuchs G, Banzer P, Rodríguez-Fortuño F J and Zayats A V 2019 Experimental demonstration of linear and spinning Janus dipoles for polarisation- and wavelength-selective near-field coupling *Light Sci. Appl.* **8** 52
- [51] Koshelev K and Kivshar Y 2021 Dielectric resonant metaphotonics *ACS Photonics* **8** 102–12
- [52] Alaei R, Rockstuhl C and Fernandez-Corbaton I 2019 Exact multipolar decompositions with applications in nanophotonics *Adv. Opt. Mater.* **7** 1800783
- [53] Kaelberer T, Fedotov V A, Papasimakis N, Tsai D P and Zheludev N I 2010 Toroidal dipolar response in a metamaterial *Science* **330** 1510–2
- [54] Ahmadivand A, Gerislioglu B, Ahuja R and Mishra Y K 2020 Terahertz plasmonics: the rise of toroidal metadevices towards immunobiosensings *Mater. Today* **32** 108–30
- [55] Ahmadivand A, Gerislioglu B, Ahuja R and Mishra Y K 2020 Toroidal metaphotonics and metadevices *Laser Photonics Rev.* **14** 1900326
- [56] Wu P C *et al* 2018 Optical anapole metamaterial *ACS Nano* **12** 1920–7
- [57] Gurvitz E A, Ladutenko K S, Dergachev P A, Evlyukhin A B, Miroshnichenko A E and Shalin A S 2019 The high-order toroidal moments and anapole states in all-dielectric photonics *Laser Photonics Rev.* **13** 1800266
- [58] Cui X, Lai Y, Ai R, Wang H, Shao L, Chen H, Zhang W and Wang J 2020 Anapole states and toroidal resonances realized in simple gold nanoplate-on-mirror structures *Adv. Opt. Mater.* **8** 2001173
- [59] Marinica D C, Borisov A G and Shabanov S V 2008 Bound states in the continuum in photonics *Phys. Rev. Lett.* **100** 183902

- [60] Hsu C W, Zhen B, Stone A D, Joannopoulos J D and Soljačić M 2016 Bound states in the continuum *Nat. Rev. Mater.* **1** 16048
- [61] Pilipchuka A S and Sadreeva A F 2017 Accidental bound states in the continuum in an open Sinai billiard *Phys. Lett. A* **381** 720–4
- [62] Krasnok A and Alú A 2018 Embedded scattering eigenstates using resonant metasurfaces *J. Opt.* **20** 064002
- [63] Yu Z, Wang Y, Sun B, Tong Y, Xu J-B, Tsang H K and Sun X 2019 Hybrid 2d-material photonics with bound states in the continuum *Adv. Opt. Mater.* **7** 1901306
- [64] Murai S, Abujetas D R, Castellanos G W, Sánchez-Gil J A, Zhang F and Rivas J G 2020 Bound states in the continuum in the visible emerging from out-of-plane magnetic dipoles *ACS Photonics* **7** 2204–10
- [65] Neale S and Muljarov E 2021 Accidental and symmetry-protected bound states in the continuum in a photonic-crystal slab: a resonant-state expansion study *Phys. Rev. B* **103** 155112
- [66] Neale S and Muljarov E 2020 Resonant-state expansion for planar photonic crystal structures *Phys. Rev. B* **101** 155128
- [67] Solnyshkov D D, Weiss T, Malpuech G and Gippius N A 2011 Polariton laser based on a ZnO photonic crystal slab *Appl. Phys. Lett.* **99** 111110
- [68] Doppler J *et al* 2016 Dynamically encircling an exceptional point for asymmetric mode switching *Nature* **537** 76–80
- [69] Langbein W 2018 No exceptional precision of exceptional-point sensors *Phys. Rev. A* **98** 023805
- [70] Wiersig J 2020 Review of exceptional point-based sensors *Photon. Res.* **8** 1457–67
- [71] Humphrey A D and Barnes W L 2014 Plasmonic surface lattice resonances on arrays of different lattice symmetry *Phys. Rev. B* **90** 075404
- [72] Tretnak V, Hohenester U, Krenn J R and Hohenau A 2020 The role of particle size in the dispersion engineering of plasmonic arrays *J. Phys. Chem. C* **124** 2104–12
- [73] Bin-Alam M S *et al* 2021 Ultra-high-Q resonances in plasmonic metasurfaces *Nat. Commun.* **12** 974
- [74] Wang B, Yu P, Wang W, Zhang X, Kuo H-C, Xu H and Wang Z M 2021 High-Q plasmonic resonances: fundamentals and applications *Adv. Opt. Mater.* **9** 2001520
- [75] Wood R W 1902 On a remarkable case of uneven distribution of light in a diffraction grating spectrum *Phil. Mag.* **4** 396–402
- [76] Rayleigh L 1907 Note on the remarkable case of diffraction spectra described by Prof. Wood *Phil. Mag.* **14** 60–65
- [77] Rayleigh L 1907 On the dynamical theory of gratings *Proc. R. Soc. A* **79** 399–416
- [78] Gamov G 1928 Zur Quantentheorie des Atomkerns *Z. Phys.* **51** 204–12
- [79] Zel'dovich Y B 1961 On the theory of unstable states *Sov. Phys. JETP* **12** 542–5
- [80] Shnol È È 1971 Remarks on the theory of quasistationary states *Theor. Math. Phys.* **8** 729–36
- [81] Sammut R and Snyder A W 1976 Leaky modes on circular optical waveguides *Appl. Opt.* **15** 477–82
- [82] Sammut R and Snyder A W 1976 Leaky modes on a dielectric waveguide: orthogonality and excitation *Appl. Opt.* **15** 1040–4
- [83] Lobanov S V, Zorinians G, Langbein W and Muljarov E A 2017 Resonant-state expansion of light propagation in nonuniform waveguides *Phys. Rev. A* **95** 053848
- [84] Upendar S, Allayarov I, Schmidt M A and Weiss T 2018 Analytical mode normalization and resonant state expansion for bound and leaky modes in optical fibers—an efficient tool to model transverse disorder *Opt. Express* **26** 22536–46
- [85] Lai H M, Leung P T, Young K, Barber P W and Hill S C 1990 Time-independent perturbation for leaking electromagnetic modes in open systems with application to resonances in microdroplets *Phys. Rev. A* **41** 5187–98
- [86] Weinstein L A 1969 *Open Resonators and Open Waveguides* (Boulder, CO: Golem Press)
- [87] Doost M B, Langbein W and Muljarov E A 2013 Resonant state expansion applied to two-dimensional open optical systems *Phys. Rev. A* **87** 043827
- [88] Bai Q, Perrin M, Sauvan C, Hugonin J P and Lalanne P 2013 Efficient and intuitive method for the analysis of light scattering by a resonant nanostructure *Opt. Express* **21** 27371–82
- [89] Kristensen P T, Ge R-C and Hughes S 2015 Normalization of quasinormal modes in leaky optical cavities and plasmonic resonators *Phys. Rev. A* **92** 053810
- [90] Muljarov E A and Langbein W 2017 Comment on “Normalization of quasinormal modes in leaky optical cavities and plasmonic resonators” *Phys. Rev. A* **96** 017801
- [91] Muljarov E A and Weiss T 2018 Resonant-state expansion for open optical systems: generalization to magnetic, chiral and bi-anisotropic materials *Opt. Lett.* **43** 1978–81
- [92] Kristensen P T, Ge R-C and Hughes S 2017 Reply to “comment on ‘normalization of quasinormal modes in leaky optical cavities and plasmonic resonators’” *Phys. Rev. A* **96** 017802
- [93] Lalanne P 2020 Mode volume of electromagnetic resonators: let us try giving credit where it is due (arXiv:2011.00218 [physics.optics])
- [94] Lalanne P, Yan W, Vynck K, Sauvan C and Hugonin J 2018 Light interaction with photonic and plasmonic resonances *Laser Photonics Rev.* **12** 1700113
- [95] Kristensen P T, Herrmann K, Intravaia F and Busch K 2020 Modelling electromagnetic resonators using quasinormal modes *Adv. Opt. Photonics* **12** 612–708
- [96] Lind P 1993 Completeness relations and resonant state expansions *Phys. Rev. C* **47** 1903–20
- [97] Lind P, Liotta R J, Maglione E and Vertse I 1994 Resonant state expansions of the continuum *Z. Phys. A* **9** 231–6
- [98] Lobanov S V, Langbein W and Muljarov E A 2019 Resonant-state expansion applied to three-dimensional open optical systems: complete set of static modes *Phys. Rev. A* **100** 063811
- [99] Haus H A and Huang W 1991 Coupled-mode theory *Proc. IEEE* **79** 1505–18
- [100] Unger A and Kreiter M 2009 Analyzing the performance of plasmonic resonators for dielectric sensing *J. Phys. Chem. C* **113** 12243–51
- [101] Gallinet B and Martin O J F 2013 Refractive index sensing with subradiant modes: a framework to reduce losses in plasmonic nanostructures *ACS Nano* **7** 6978–87
- [102] Upendar S, Schmidt M A and Weiss T 2021 What optical fiber modes reveal: group velocity and effective index for external perturbations *J. Opt. Soc. Am. B* **38** 1097–103
- [103] Hergert G, Vogelsang J, Schwarz F, Wang D, Kollmann H, Groß P, Lienau C, Runge E and Schaaf P 2017 Long-lived electron emission reveals localized plasmon modes in disordered nanosponge antennas *Light Sci. Appl.* **6** e17075
- [104] Silver S 1949 *Radiation From Current Distributions* (New York: McGraw-Hill)
- [105] Akimov A B, Gippius N A and Tikhodeev S G 2011 Optical Fano resonances in photonic crystal slabs near diffraction threshold anomalies *JETP Lett.* **93** 427–30
- [106] Defrance J and Weiss T 2020 On the pole expansion of electromagnetic fields *Opt. Express* **28** 32363–76
- [107] Lalanne P *et al* 2019 Quasinormal mode solvers for resonators with dispersive materials *J. Opt. Soc. Am. A* **36** 686–704
- [108] Arfken G B and Weber H J 2011 *Mathematical Methods for Physicists* 6th edn (London: Elsevier)

- [109] Asadchy V S, Mirmoosa M S, Díaz-Rubio A, Fan S and Tretyakov S A 2020 Tutorial on electromagnetic nonreciprocity and its origins *Proc. IEEE* **108** 1684–727
- [110] Onsager L 1931 Reciprocal relations in irreversible processes. I *Phys. Rev.* **37** 405–26
- [111] Onsager L 1931 Reciprocal relations in irreversible processes. II *Phys. Rev.* **38** 2265–79
- [112] Casimir H B G 1945 On Onsager's principle of microscopic reversibility *Rev. Mod. Phys.* **17** 343–50
- [113] Allayarov I, Upendar S, Schmidt M A and Weiss T 2018 Analytic mode normalization for the Kerr nonlinearity parameter: prediction of nonlinear gain for leaky modes *Phys. Rev. Lett.* **121** 213905
- [114] Allayarov I, Schmidt M A and Weiss T 2020 Theory of four-wave mixing for bound and leaky modes *Phys. Rev. A* **101** 043806
- [115] Zolla F, Nicolet A and Demésy G 2018 Photonics in highly dispersive media: the exact modal expansion *Opt. Lett.* **43** 5813–6
- [116] Truong M D, Demésy G, Zolla F and Nicolet A 2020 Quasi-normal mode (DQNM) expansion in open and periodic nanophotonic structures 2019 22nd Int. Conf. Computation of Electromagnetic Fields (COMPUMAG) vol 29 pp 29016–32
- [117] Truong M D, Nicolet A, Demésy G and Zolla F 2020 A continuous family of exact dispersive quasi-normal modal (DQNM) expansions for dispersive photonic structures *Opt. Express* **29** 29016–32
- [118] Keldysh M V 1951 On eigenvalues and eigenfunctions of some classes of non self-adjoint equations *Dokl. Akad. Nauk SSSR* **77** 11–14
- [119] Keldysh M V 1971 On the completeness of the eigenfunctions of some classes of non-selfadjoint linear operators *Russ. Math. Surv.* **26** 15
- [120] Sehmi H S, Langbein W and Muljarov E A 2017 Optimizing the Drude–Lorentz model for material permittivity: method, program and examples for gold, silver and copper *Phys. Rev. B* **95** 115444
- [121] Colom R, Mcphedran R, Stout B and Bonod N 2018 Modal expansion of the scattered field: causality, nondivergence and nonresonant contribution *Phys. Rev. B* **98** 085418
- [122] Gérard J M 2003 Solid-state cavity-quantum electrodynamics with self-assembled quantum dots *Single Quantum Dots (Topics in Applied Physics)* vol 90 (Berlin: Springer)
- [123] Koenderink A F 2010 On the use of Purcell factors for plasmon antennas *Opt. Lett.* **35** 4208–10
- [124] Vertse T, Curutchet P and Liotta R J 1989 The use of Gamow functions in nuclear problems *Resonances The Unifying Route Towards the Formulation of Dynamical Processes Foundations and Applications in Nuclear, Atomic and Molecular Physics (Lecture Notes in Physics)* vol 325, ed E Brändas and N Elander (Berlin: Springer)
- [125] Hugonin J P and Lalanne P 2005 Perfectly matched layers as nonlinear coordinate transforms: a generalized formalization *J. Opt. Soc. Am. A* **22** 1844–9
- [126] Mcphedran R C and Stout B 2020 Killing Mie softly: analytic integrals for complex resonant states *Q. J. Mech. Appl. Math.* **73** 119–39
- [127] Weiss T, Granet G, Gippius N A, Tikhodeev S G and Giessen H 2009 Matched coordinates and adaptive spatial resolution in the Fourier modal method *Opt. Express* **17** 8051–61
- [128] Weiss T, Gippius N A, Tikhodeev S G, Granet G and Giessen H 2011 Derivation of plasmonic resonances in the Fourier modal method with adaptive spatial resolution and matched coordinates *J. Opt. Soc. Am. A* **28** 238–44
- [129] Perrin M 2016 Eigen-energy effects and non-orthogonality in the quasi-normal mode expansion of Maxwell equations *Opt. Express* **24** 27137–51
- [130] Unger G, Trügler A and Hohenester U 2018 Novel modal approximation scheme for plasmonic transmission problems *Phys. Rev. Lett.* **121** 246802
- [131] Gras A, Lalanne P and Duruflé M 2020 Non-uniqueness of the quasi-normal mode expansion of electromagnetic Lorentz-dispersive materials *J. Opt. Soc. Am. A* **37** 1219–28
- [132] García-Calderón G 1982 On the over-completeness of the set of bound, antibound and resonant states *Let. Nuovo Cimento* **33** 253–7
- [133] Li L 1996 Use of Fourier series in the analysis of discontinuous periodic structures *J. Opt. Soc. Am. A* **13** 1870–6
- [134] Li L 1997 New formulation of the Fourier modal method for crossed surface-relief gratings *J. Opt. Soc. Am. A* **14** 2758–67
- [135] Granet G 1999 Reformulation of the lamellar grating problem through the concept of adaptive spatial resolution *J. Opt. Soc. Am. A* **16** 2510–6
- [136] Li L 2003 Fourier modal method for crossed anisotropic gratings with arbitrary permittivity and permeability tensors *J. Opt. A: Pure Appl. Opt.* **5** 345–55
- [137] Binkowski F, Betz F, Colom R, Hammerschmidt M, Zschiedrich L and Burger S 2020 Quasinormal mode expansion of optical far-field quantities *Phys. Rev. B* **102** 035432
- [138] Both S, Schäferling M, Sterl F, Muljarov E A, Giessen H and Weiss T 2021 Nanophotonic chiral sensing: how does it actually work? (arXiv:2106.15699 [physics.optics])
- [139] Mie G 1908 Beiträge zur optik trüber medien, speziell kolloidaler metallösungen *Ann. Phys., Lpz.* **25** 377–445
- [140] Grigoriev V, Tahri A, Varault S, Rolly B, Stout B, Wenger J and Bonod N 2013 Optimization of resonant effects in nanostructures via Weierstrass factorization *Phys. Rev. A* **88** 011803(R)
- [141] Gippius N A, Tikhodeev S G and Ishihara T 2005 Optical properties of photonic crystal slabs with an asymmetrical unit cell *Phys. Rev. B* **72** 45138-1-7
- [142] Zschiedrich L, Binkowski F, Nikolay N, Benson O, Kewes G and Burger S 2018 Riesz-projection-based theory of light-matter interaction in dispersive nanoresonators *Phys. Rev. A* **98** 043806
- [143] Limonov M F, Rybin M V, Poddubny A N and Kivshar Y S 2017 Fano resonances in photonics *Nat. Photon.* **11** 543–54
- [144] Miroshnichenko A E, Flach S and Kivshar Y S 2010 Fano resonances in nanoscale structures *Rev. Mod. Phys.* **82** 2257–98
- [145] Luk'yanchuk B, Zheludev N I, Maier S A, Halas N J, Nordlander P, Giessen H and Chong C T 2010 The fano resonance in plasmonic nanostructures and metamaterials *Nat. Mater.* **9** 707–15
- [146] Gallinet B and Martin O J F 2011 Relation between near-field and far-field properties of plasmonic fano resonances *Opt. Express* **19** 22167–75
- [147] Bekele D, Yu Y, Yvind K and Mork J 2019 In-plane photonic crystal devices using fano resonances *Laser Photonics Rev.* **13** 1900054
- [148] Papasimakis N, Fedotov V A, Zheludev N I and Prosvirnin S L 2008 Metamaterial analog of electromagnetically induced transparency *Phys. Rev. Lett.* **101** 253903
- [149] Liu N, Langguth L, Weiss T, Kästel J, Fleischhauer M, Pfau T and Giessen H 2009 Plasmonic electromagnetically induced transparency at the Drude damping limit *Nat. Mater.* **8** 758–62
- [150] Liu N, Weiss T, Mesch M, Langguth L, Eigenthaler U, Hirscher M, Sönnichsen C and Giessen H 2010 Planar

- metamaterial analogue of electromagnetically induced transparency for plasmonic sensing *Nano Lett.* **10** 1103–7
- [151] Muljarov E A 2020 Full electromagnetic Green's dyadic of spherically symmetric open optical systems and elimination of static modes from the resonant-state expansion *Phys. Rev. A* **101** 053854
- [152] Liu N, Mesch M, Weiss T, Hentschel M and Giessen H 2010 Infrared perfect absorber and its application as plasmonic sensor *Nano Lett.* **10** 2342–8
- [153] Yoo S and Park Q-H 2019 Metamaterials and chiral sensing: a review of fundamentals and applications *Nanophotonics* **8** 249–61
- [154] Yesilkoy F, Arvelo E R, Jahani Y, Liu M, Tittel A, Cevher V, Kivshar Y and Altug H 2019 Ultrasensitive hyperspectral imaging and biodetection enabled by dielectric metasurfaces *Nat. Photon.* **13** 390–6
- [155] Sterl F, Strohfeldt N, Both S, Herkert E, Weiss T and Giessen H 2020 Design principles for sensitivity optimization in plasmonic hydrogen sensors *ACS Sens.* **5** 917–27
- [156] Johnson S G, Ibanescu M, Skorobogatiy M A, Weisberg O, Joannopoulos J D and Fink Y 2002 Perturbation theory for maxwell's equations with shifting material boundaries *Phys. Rev. E* **65** 066611
- [157] Yan W, Lalanne P and Qiu M 2020 Shape deformation of nanoresonator: a quasinormal-mode perturbation theory *Phys. Rev. Lett.* **125** 013901
- [158] Cohen-Tannoudji C 1991 *Quantum Mechanics* (Paris: Hermann)
- [159] Almousa S F and Muljarov E A 2021 Varying the medium surrounding an optical resonator: an efficient and rigorous way to calculate its spectral changes (arXiv:2109.07026 [physics.optics])
- [160] Etchegoin P G, Le Ru E C and Meyer M 2006 An analytic model for the optical properties of gold *J. Chem. Phys.* **125** 164705-1–3
- [161] Nesterov M L, Yin X, Schäferling M, Giessen H and Weiss T 2016 The role of plasmon-generated near fields for enhanced circular dichroism spectroscopy *ACS Photonics* **4** 578–83
- [162] Dung H T, Knöll L and Welsch D-G 2000 Spontaneous decay in the presence of dispersing and absorbing bodies: general theory and application to a spherical cavity *Phys. Rev. A* **62** 053804
- [163] Dung H T, Knöll L and Welsch D-G 2001 Decay of an excited atom near an absorbing microsphere *Phys. Rev. A* **64** 013804
- [164] Curto A G, Volpe G, Taminiau T H, Kreuzer M P, Quidant R and van Hulst N F 2010 Unidirectional emission of a quantum dot coupled to a nanoantenna *Science* **329** 930–3
- [165] Akselrod G M, Argyropoulos C, Hoang T B, Ciraci C, Fang C, Huang J, Smith D R and Mikkelsen M H 2014 Probing the mechanisms of large Purcell enhancement in plasmonic nanoantennas *Nat. Photon.* **8** 835–40
- [166] Zhan P, Urban M J, Both S, Duan X, Kuzyk A, Weiss T and Liu N 2019 DNA-assembled nanoarchitectures with multiple components in regulated and coordinated motion *Sci. Adv.* **5** eaax6023
- [167] Herzog T, Böhrkircher S, Both S, Fischer M, Sittig R, Jetter M, Portalupi S L, Weiss T and Michler P 2020 Realization of a tunable fiber-based double cavity system *Phys. Rev. B* **102** 235306
- [168] Cai Y-Y *et al* 2019 Single-particle emission spectroscopy resolves d-hole relaxation in copper nanocubes *ACS Energy Lett.* **4** 2458–65
- [169] Ostovar B, Cai Y-Y, Tauzin L J, Lee S A, Ahmadvand A, Zhang R, Nordlander P and Link S 2020 Increased intraband transitions in smaller gold nanorods enhance light emission *ACS Nano* **14** 15757–65
- [170] Solntsev A S, Agarwal G S and Kivshar Y S 2021 Metasurfaces for quantum photonics *Nat. Photon.* **15** 327–36
- [171] Wei H, Yan X, Niu Y, Li Q, Jia Z and Xu H 2021 Plasmon–exciton interactions: spontaneous emission and strong coupling *Adv. Funct. Mater.* **2100889**
- [172] Purcell E M 1946 Spontaneous emission probabilities at radio frequencies *Phys. Rev.* **69** 681
- [173] Coccioli R, Boroditsky M, Kim K W, Rahmat-Samii Y and Yablonovitch E 1998 Smallest possible electromagnetic mode volume in a dielectric cavity *IEEE Proc. J* **145** 391–7
- [174] Joannopoulos J D, Johnson S G, Winn J N and Meade R D 2008 *Photonic Crystals: Molding the Flow of Light* 2nd edn (Princeton, NJ: Princeton University Press)
- [175] Leung P T, Liu S Y and Young K 1994 Completeness and orthogonality of quasinormal modes in leaky optical cavities *Phys. Rev. A* **49** 3057–67
- [176] Leung P T and Pang K M 1996 Completeness and time-independent perturbation of morphology-dependent resonances in dielectric spheres *J. Opt. Soc. Am. B* **13** 805–17
- [177] Lee K M, Leung P T and Pang K M 1999 Dyadic formulation of morphology-dependent resonances. I. Completeness relation *J. Opt. Soc. Am. B* **16** 1409–17
- [178] Franke S, Hughes S, Dezfouli M K, Kristensen P T, Busch K, Knorr A and Richter M 2019 Quantization of quasinormal modes for open cavities and plasmonic cavity quantum electrodynamics *Phys. Rev. Lett.* **122** 213901
- [179] Zambrana-Puyalto X and Bonod N 2015 Purcell factor of spherical MIE resonators *Phys. Rev. B* **91** 195422
- [180] Wu T, Gurioli M and Lalanne P 2021 Nanoscale light confinement: the Q's and V's *ACS Photonics* **8** 1522–38
- [181] Novotny L and Hecht B 2012 *Principles of Nano-Optics* 2nd edn (Cambridge: Cambridge University Press)
- [182] Dezfouli M K and Hughes S 2018 Regularized quasinormal modes for plasmonic resonators and open cavities *Phys. Rev. B* **97** 115302
- [183] Caselli N, Wu T, Arregui G, Granchi N, Intonti F, Lalanne P and Gurioli M 2021 Near-field imaging of magnetic complex mode volume *ACS Photonics* **8** 1258–63
- [184] Bergman D J 1979 Dielectric constant of a two-component granular composite: a practical scheme for calculating the pole spectrum *Phys. Rev. B* **19** 2359
- [185] Bergman D J 1979 The dielectric constant of a simple cubic array of identical spheres *J. Phys. C: Solid State Phys.* **12** 4947
- [186] Bergman D J and Stroud D 1980 Theory of resonances in the electromagnetic scattering by macroscopic bodies *Phys. Rev. B* **22** 3527
- [187] Farhi A and Bergman D J 2016 Electromagnetic eigenstates and the field of an oscillating point electric dipole in a flat-slab composite structure *Phys. Rev. A* **93** 063844
- [188] Jackson J D 1999 *Classical Electrodynamics* 3rd edn (New York: Wiley)
- [189] Chen P Y, Bergman D J and Sivan Y 2019 Generalizing normal mode expansion of electromagnetic Green's tensor to open systems *Phys. Rev. Appl.* **11** 044018
- [190] Chen P Y, Sivan Y and Muljarov E A 2020 An efficient solver for the generalized normal modes of non-uniform open optical resonators *J. Comput. Phys.* **422** 109754
- [191] Chen P Y and Sivan Y 2021 Resolving the Gibbs phenomenon via a discontinuous basis in a mode solver for open optical systems *J. Comput. Phys.* **429** 110004
- [192] Pascale M, Miano G, Tricarico R and Forestiere C 2019 Full-wave electromagnetic modes and hybridization in nanoparticle dimers *Sci. Rep.* **9** 14524

- [193] Prodan E, Radloff C, Halas N J and Nordlander P 2003 A hybridization model for the plasmon response of complex nanostructures *Science* **302** 419–22
- [194] Prodan E and Nordlander P 2004 Plasmon hybridization in spherical nanoparticles *J. Chem. Phys.* **120** 5444–54
- [195] Gippius N A, Weiss T, Tikhodeev S G and Giessen H 2010 Resonant mode coupling of optical resonances in stacked nanostructures *Opt. Express* **18** 7569–74
- [196] Vial B and Hao Y 2016 A coupling model for quasi-normal modes of photonic resonators *J. Opt.* **18** 115004
- [197] Tao C, Zhu J, Zhong Y and Liu H 2020 Coupling theory of quasinormal modes for lossy and dispersive plasmonic nanoresonators *Phys. Rev. B* **102** 045430
- [198] Li Q, Wu T, van de Groep J, Lalanne P and Brongersma M L 2021 Structural color from a coupled nanowire pair beyond the bonding and antibonding model *Optica* **8** 464–70
- [199] Weiss T, Gippius N A, Granet G, Tikhodeev S G, Taubert R, Fu L, Schweizer H and Giessen H 2011 Strong resonant mode coupling of Fabry–Perot and grating resonances in stacked two-layer systems *Photon. Nanostruct.: Fundam. Appl.* **9** 390–7
- [200] Weiss T, Wong G K L, Biancalana F, Barnett S M, Xi X M and 2013 P. St.J. Russell. Topological Zeeman effect and circular birefringence in twisted photonic crystal fibers *J. Opt. Soc. Am. B* **30** 2921–7
- [201] Snyder A W and Love J 1983 *Optical Waveguide Theory* (London: Chapman and Hall)
- [202] Agrawal G 2001 *Nonlinear Fiber Optics* 3rd edn (San Diego, CA: Academic)
- [203] Maslov A V 2014 Rigorous calculation of the nonlinear Kerr coefficient for a waveguide using power-dependent dispersion modification *Opt. Lett.* **39** 4396–9
- [204] Li G, de Sterke C M and Palomba S 2017 General analytic expression and numerical approach for the Kerr nonlinear coefficient of optical waveguides *Opt. Lett.* **42** 1329–32
- [205] Elsayw M M and Renversez G 2018 Exact calculation of the nonlinear characteristics of 2D isotropic and anisotropic waveguides *Opt. Lett.* **43** 2446–9
- [206] Boyd R W 2003 *Nonlinear Optics* 2nd edn (San Diego, CA: Academic)
- [207] Paul T, Rockstuhl C and Lederer F 2010 A numerical approach for analyzing higher harmonic generation in multilayer nanostructures *J. Opt. Soc. Am. B* **27** 1118–30
- [208] Paul T, Rockstuhl C and Lederer F 2010 Integrating cold plasma equations into the Fourier modal method to analyze second harmonic generation at metallic nanostructures *J. Mod. Opt.* **58** 438–48
- [209] DeFrance J, Schäferling M and Weiss T 2020 Modeling of second-harmonic generation in periodic nanostructures by the Fourier modal method with matched coordinates *Opt. Express* **26** 13746–58
- [210] Gigli C, Wu T, Marino G, Borne A, Leo G and Lalanne P 2020 Quasinormal-mode non-Hermitian modeling and design in nonlinear nano-optics *ACS Photonics* **7** 1197–205
- [211] Christopoulos T, Tsilipakos O and Kriezis E E 2020 Perturbation theory for Kerr nonlinear leaky cavities *Opt. Lett.* **45** 6442–5
- [212] Dirac P A M 1988 *The Principles of Quantum Mechanics* (Oxford: Oxford University Press)
- [213] Dirac P A M 1963 The evolution of the physicist's picture of nature *Sci. Am.* **208** 45–53
- [214] Feynman R 1985 *The Character of Physical Law* (Cambridge, MA: MIT Press)
- [215] Tanimu A and Muljarov E A 2018 Resonant-state expansion applied to one-dimensional quantum systems *Phys. Rev. A* **98** 022127
- [216] Primo A G, Carvalho N C, Kersul C M, Frateschi N C, Wiederhecker G S and Mayer-Alegre T P 2020 Quasinormal-mode perturbation theory for dissipative and dispersive optomechanics *Phys. Rev. Lett.* **125** 233601